INFRARED PHOTOMETRY OF METAL RICH GALACTIC GLOBULAR CLUSTERS

JUDITH G. COHEN AND CELESTE SLEEPER
Palomar Observatory, California Institute of Technology, Mail Code 105-24, Pasadena, California 91125
Electronic mail: jlc@astro.caltech.edu, ecs@stro.caltech.edu

Received 1994 July 1; revised 1994 September 7

ABSTRACT

Infrared photometry is presented for the giant branches of five galactic globular clusters, including three very metal rich ones located near the galactic center. New visual photometry was required for three of these objects. The metallicities of these clusters as inferred from the dereddened colors of their giant branches are in reasonable agreement with those inferred by spectroscopy of the integrated light of these systems. The spread in color seen along the giant branches of the most highly reddened of these globular clusters is shown to be consistent with patchy interstellar reddening. Abundance variations within a cluster are not required to explain the observations. The range of metallicity is confined to less than 0.2 dex in NGC 5927, and to 0.1 dex in NGC 7099. The spread in $V-K$ color is a strong constraint on abundance variations within a globular cluster.

1. INTRODUCTION

The very metal rich galactic globular clusters comprise a group of poorly studied objects. They often have high foreground reddening, suffer severe crowding because they are located near the galactic center, and may have serious field star contamination. In many cases, the only available optical photometry is old photographic photometry. We have obtained new infrared photometry using an array detector of the giant branch stars in several of these clusters (and in two cases, new optical photometry as well) with the following goals. First we would like to confirm, based on the location of their giant branches, the estimates of the high metallicity of these clusters. Second we would like to determine whether the large apparent scatter in the existing optical color magnitude diagrams is due to poor photometry, an internal metallicity dispersion, or reddening variations. We would also like to check on the luminosity of the brightest red giant, which defines the luminosity of the helium flash and can be used as a check on the cluster distance. Finally, we would like to analyze the luminosity variances of these globular clusters in the infrared.

We have picked a sample of galactic globular clusters with metallicities at least twice that of 47 Tuc based on the compendium of Zinn & West (1984), with $E(B-V)\leq 0.6$ mag, a distance not larger than 10 kpc, and v_r significantly different from 0 km s^{-1}, so that if necessary, field stars can easily be separated from cluster members using radial velocity measurements. The three program clusters are NGC 5927, NGC 6624, and NGC 6528. Two other clusters, NGC 6171 and NGC 7099, were also observed in the infrared. As initial values to guide us, we use the metallicities of Zinn & West (1984), updated by Armandroff & Zinn (1988). We use the values of $E(B-V)$ and apparent visual brightness of the horizontal branch at the color of the RR Lyrae gap tabulated by Peterson (1993).

2. OBSERVATIONS

The advantages of using an infrared array detector for investigation of the giant branch of highly reddened galactic globular clusters are obvious. Davidge & Simons (1991), who studied M69 in this way, review the major points. See also Davidge *et al.* (1992). For our observations, we have used the Rockwell Nicmos 3 infrared array camera described in Persson *et al.* (1992) at the Cassegrain focus of the 40 in. Swope telescope at the Las Campanas Observatory in Chile for five nights in June 1992. This array has 256×256 pixels, covering 0.45 arcsec/pixel or a square 116 arcsec on a side. The seeing at K was 1.0 to 1.5 arcsec. Observations were made at J and at K only. The fainter standards of Elias *et al.* (1982) were used. Multiple short exposures (60 and 120 s at J, and 30 and 60 s at K) were obtained for the globular cluster fields, typically with six images at each exposure time taken at each positional setting. Every field was observed at three positional settings, each slightly offset from the others on the sky, to help minimize variations arising from flatfielding problems. Two different fields were observed in most of these globular clusters. These were chosen to avoid the extreme crowding of the core of the cluster, while not being so far from the center that field star contamination becomes serious.

We slightly modified IRAF scripts originally written by Eric Persson to linearize the frames, collect the multiple exposures at each position, remove the dark signal, flatten the data using dome flats, process the standard stars, and make mosaics of the globular cluster data in J and in K. Once this was accomplished, we reversed to using FIGARO as the data analysis package. DAOPHOT (Stetson 1987) was used to determine magnitudes from each of the three positional settings for each field. The σ values given here are those of the multiple measurements of J or K magnitude for each object; they are not computed from the signal and sky values for a measured magnitude.

Saturation of the central pixel of stellar images occurs on

 0004-6256/95/109(1)/242/22/$0.90

TABLE 1. *V* and *R* photometry for NGC 5927.

x (pixels)	y (pixels)	Star ID	V(CTIO) (mag)	Δ (V) (mag)	V−R (mag)	x (pixels)	y (pixels)	Star ID	V(CTIO) (mag)	Δ (V) (mag)	V−R (mag)
345	123		15.53		0.47	524	124		15.30		1.07
180	146	1− 436	17.19	0.03	0.84	204	148	2− 873	16.41	0.04	0.98
276	148	2− 884	16.08	−0.10	0.71	452	154		17.13		0.78
104	156	1− 445	16.13	−0.43	0.60	156	162	1− 439	16.54	0.02	0.82
484	166		16.94		0.84	111	169	1− 447	16.57	−0.23	0.80
264	171	2− 888	16.59	0.02	0.79	113	177	1− 448	16.44	−0.25	0.92
265	177	2− 889	17.17	0.05	0.72	312	177	2− 886	15.02	0.01	1.13
106	179	1− 449	17.02	−0.35	0.81	335	183	3− 907	16.75	0.11	0.86
159	185	1− 463	16.58	−0.08	0.77	127	194		16.62		0.91
190	194		15.42		0.98	169	196		16.15		0.76
184	199	1− 467	17.01	−0.05	0.78	192	206	1− 468	16.33	−0.04	0.87
390	210	3− 904	16.72	0.00	0.80	106	214	1− 459	16.61	−0.25	0.83
129	213	1− 476	16.54	−0.18	0.80	288	213	2− 892	15.68	−0.02	0.80
142	215	1− 474	17.12	−0.13	0.79	298	215	2− 893	17.10	0.08	0.78
460	216		13.27		0.76	440	219	3− 902	17.32	0.07	0.80
153	225	1− 472	15.87	−0.29	0.98	145	227	1− 473	14.74	−0.23	1.26
231	229	2− 891	15.05	−0.21	0.98	117	229	1− 477	16.59	−0.19	0.80
176	233	1− 471	17.28	−0.07	0.86	286	233	2− 897	16.46	0.09	0.76
96	234	1− 479	16.52	−0.43	0.80	469	234		15.06		0.42
490	235		16.01		0.57	526	235		14.94		0.71
374	236	3−1294	14.81	0.03	0.96	216	244	2− 501	15.27	−0.06	0.48
111	246	1− 5	16.62	−0.17	0.77	98	248	1− 1	16.85	−0.27	0.82
472	251		15.67		0.67	186	252	1− 10	16.68	0.00	0.81
105	253	1− 3	16.52	−0.27	0.79	114	258	1− 4	15.01	−0.65	0.79
490	258		15.60		0.50	97	261	1− 2	16.19	−0.55	0.84
156	269	1− 23	15.47	−0.20	1.05	195	271	1− 17	15.94	−0.09	0.82
253	279	2− 516	16.56	0.01	0.80	86	282		16.08		0.74
393	285	3−1287	17.26	−0.01	0.85	55	288		17.15		0.86
216	289		16.07		0.82	109	289		15.36		0.94
170	288	1− 21	17.18	−0.06	0.83	254	289	2− 517	16.61	−0.04	0.80
93	289		16.71		0.83	127	293	1− 29	16.71	−0.17	0.83
176	298	1− 18	16.58	−0.18	0.75	259	297	2− 519	16.84	−0.01	0.77
70	299		16.20		0.81	75	300		16.82		0.84
96	301	1− 33	16.27	−0.34	0.81	206	301		16.44		0.80
225	303	2− 522	16.48	−0.03	0.79	247	304	2− 521	13.66	−0.25	0.92
160	306	1− 40	15.76	−0.26	0.91	53	308		16.47		0.83
66	308		16.55		0.80	167	308	1− 41	16.43	−0.29	0.77
469	308		15.81		0.90	193	311	1− 44	16.77	−0.02	0.86
247	304		13.66		0.92	518	311		16.37		0.58
93	312		16.04		0.68	248	312		16.31		0.70
124	313	1− 36	17.30	−0.14	0.79	92	316		16.05		0.68
64	318		17.11		0.83	224	317	2− 523	16.59	−0.05	0.79
181	320	1− 43	17.33	−0.05	0.85	54	322		16.65		0.80
435	322	3−1274	15.96	−0.06	0.85	74	323		16.51		0.76
153	325	1− 38	15.64	−0.21	0.90	61	328		16.68		0.82
264	328	2− 525	16.55	−0.04	0.78	413	328	3−1276	15.54	−0.02	0.76
256	329	2− 524	16.61	−0.07	0.79	348	330	3−1278	16.31	0.02	0.65
134	331	1− 37	15.83	−0.06	0.92	262	336	2− 530	16.21	−0.27	0.56
180	337	1− 49	16.74	0.01	0.80	87	342	1− 66	16.43	−0.35	0.78
123	342	1− 59	16.70	−0.12	0.79	78	343	1− 67	16.67	−0.33	
268	350	2− 531	16.36	−0.03	0.77	102	351	1− 65	14.94	−0.30	1.08
73	352	1− 68	15.91	−0.65	0.66	57	354		16.45		0.77
90	355	1− 69	15.60	−0.39	0.97	247	356	2− 532	14.73	−0.14	1.22
230	356	2− 533	15.16	−0.05	0.83	119	357	1− 61	17.29	−0.11	0.81
134	360	1− 56	16.59	−0.01	0.77	366	361	3−1269	16.86	0.05	0.84
324	363	3−1267	16.02	0.02	0.95	87	367	1− 70	16.99	−0.20	0.85
184	369	2− 534	16.85	−0.06	0.85	251	373		14.84		1.15
218	374	2− 536	15.18	0.01	1.03	344	376	3−1268	17.27	0.03	0.83
263	379	2− 540	15.79	−0.10	0.59	279	379	2− 541	16.66	0.05	0.78
129	386		15.42		0.99	249	384	2− 539	15.20	−0.23	1.10
85	387	1− 86	15.55	−0.38	0.98	238	390	2− 537	17.10	0.01	0.82
116	392	1− 74	12.83	−0.29	0.82	99	403	1− 84	15.56	−0.21	0.96
311	408	3−1265	15.01	0.01	0.87	164	410	2− 549	16.70	0.04	0.91
199	421	2− 550	16.85	0.05	0.87	123	422	1− 77	17.05		0.79
262	429	2− 544	16.73		0.80	209	430		16.77		0.81
94	432	1− 111	14.55		0.91	282	444		16.95		0.76
161	447	2− 557	16.56	−0.01	0.76	68	450	V−5	14.96		1.62
333	450	3−1254	14.78	−0.29	0.79	122	452	2− 559	16.65	−0.05	0.78
325	456	3−1253	14.23	−0.22	0.79	309	465		16.78		0.81
142	467		13.52		0.87	56	475	V−6	14.91		1.53
106	478	2− 563	15.94	−0.07	0.95	139	482		17.12		0.76
259	483	3−1248	16.77	0.04	0.81	87	485	2− 584	16.51	−0.26	0.69
312	490	3−1244	16.59	0.02	0.76	265	500	3−1246	16.63	0.04	0.79
136	506	2− 571	16.70		0.77	79	510	2− 582	15.27	−0.06	0.84
315	512	3−1242	16.67	0.05	0.75	215	515	3−1235	16.65	0.10	0.83
63	516	2− 580	16.52	0.00	0.81	183	516	2− 569	16.73		0.76
255	521	3−1238	15.76	0.04	1.01	281	523		16.53		0.62
126	533	2− 573	16.24		0.81	171	541		16.29		0.90
97	558		16.65		0.77	184	563		15.67		0.57
72	570		15.77		0.97	90	580		17.22		0.74
210	582		13.00		0.62						

the shortest J frames at $\approx$10.0 mag and for the shortest K frames at $\approx$8.7 mag.

3. INDIVIDUAL CLUSTERS

3.1 NGC 5927

NGC 5927 is a very metal rich globular cluster located at a distance of 8 kpc about 35° from the galactic center in the galactic plane. We have adopted $E(B-V)=0.46$ mag. Visual photometry by Menzies (1974) established that the reddening was patchy. Our two fields are centered in the region which he described as "apparently uniformly reddened" with $E(B-V)=0.52$ mag. To supplement this rather old visual photometry, CCD frames were obtained through the V and R filters at the Yale 1.0 m telescope at CTIO in July 1993 using service observing. The data were reduced in standard ways (FIGARO and DAOPHOT) described above and the results are given in Table 1. The major purpose of the Tololo photometry was to obtain additional V magnitudes for stars observed in the infrared, but it also served to confirm the estimate of the magnitude level of the red horizontal branch, which was 16.55 ± 0.08 mag from the new data, and is given as 16.60 mag by Menzies (1974).

The globular cluster distance scale we are using assumes $M_V(\mathrm{HB})=0.16[\mathrm{Fe/H}]+1.02$, from Jones *et al.* (1992). The variation of absolute magnitude of the RR Lyraes as a function of metallicity they deduce by collating all available Baade–Wesslink analyses of field RR Lyrae variables gives results comparable to other techniques. Various authors (Cohen 1992; Liu & Janes 1990; for example) have demonstrated that globular cluster RR Lyrae variables follow the same relationships between absolute V magnitude and metallicity or between absolute K magnitude and period as have been demonstrated to hold for field stars. The exact choice of a globular cluster distance scale from among the various possibilities currently in fashion does not affect the results of this paper in a substantive way, since we are to first order comparing the measured parameters of the sample globular clusters against those of calibrating globular clusters whose properties are well determined.

Table 2 lists the measurements at J and at K for NGC 5927. The first two columns give x and y in pixels, where positive y corresponds (approximately) to north and positive x to west. Then follow the observed J and K magnitudes, with dispersions given if there was more than one measurement. The dispersions between infrared magnitudes of a star as measured on multiple frames are significantly larger than those predicted purely from the statistics of the photometry on any individual frame. The final columns give the optical identification number from Menzies (1974), if optical photometry is available for that star.

Because of our small fields, we have only six stars in common with the early study of Frogel *et al.* (1983a), who observed the brightest and reddest stars over the entire cluster based on the Menzies (1974) photometry. Ignoring two variable stars, for the four remaining stars in common, we find a systematic difference of 0.03 ± 0.02 mag in J and 0.08 ± 0.04 mag in K, with our magnitudes being fainter.

Kuchinski *et al.* (1994) also obtained new infrared photometry for this cluster with the 2.5 m telescope at Las Campanas Observatory. We have 43 stars in common, and ignoring one with a large discrepancy which is probably affected by crowding, the mean difference in the $J-K$ color is 0.024 mag, with $\sigma=0.10$ mag, while the mean difference in the K magnitudes is -0.001, with $\sigma=0.12$ mag. This is a very encouraging comparison of two independent data sets.

Figures 1(a) and 1(b) show the $J-K$ and V-K colors as a function of K magnitude. Open circles denote stars without optical photometry, while filled circles denote those stars with optical photometry. The two brightest stars in the infrared denoted by open triangles are the extremely red variables V5 and V6. In an optical color–magnitude diagram, the upper end of the giant branch, particularly the red variables, would turn over towards fainter magnitudes for the reddest stars (see, for example, Ortolani *et al.* 1991b,a), while this does not happen in Fig. 1. The same phenomenon occurs to an even greater extent in NGC 6624 and also in NGC 6553 (Davidge & Simons 1994), both very metal rich globular clusters. We believe it is due to the anomalous colors and unexpected faintness at visual wavelengths of very metal rich cool giants due to large molecular blanketing.

The clump of stars somewhat blueward of the giant branch of NGC 5927 at $K_0\approx13.1$ mag is presumably the horizontal branch. This feature is much clearer in Kuchinski *et al.*'s data.

3.2 NGC 6528

NGC 6528 is a very metal rich globular cluster located in Baade's window near the galactic center. The Zinn & West (1984) metallicity of $[\mathrm{Fe/H}]=+0.12$ dex is significantly larger than that of Armandroff & Zinn (1988), who give reasons why the latter value is to be preferred. B, V visual photometry is given by van den Bergh & Younger (1979). CCD photometry at B, V, R, and I is given by Ortolani *et al.* (1991b). Although Ortolani *et al.* (1991a,b) did not publish the details of their measurements, they kindly sent them to us. Ortolani *et al.* deduce $E(B-V)=0.55$ mag, with differential reddening of up to $\Delta E(B-V)=0.33$ mag across the face of the cluster, and a distance of 7.5 kpc. Note that their measured location of the horizontal branch is $\approx$0.4 mag fainter than that obtained by van den Bergh & Younger (1979), where the HB was near the limit of their photometry. Using our assumed $M_V(\mathrm{HB})$ with Ortolani *et al.*'s $V_{\mathrm{HB}}=17.1$ mag, we deduce a distance modulus of 14.42 mag.

The cluster is confined to a small field on the sky. Thus, a single field centered on the globular cluster was observed on two different nights. A background field 400 arcsec to the east of the cluster center was observed on the same two nights. Table 3 lists the measurements of J and at K for NGC 6528. The format is identical to Table 2. The identifications are from van den Bergh & Younger (1979), or if not included there, from Ortolani's list. The V magnitudes are from Ortolani's list. There is no previous infrared photometry for any stars in this globular cluster.

Figures 2(a) and 2(b) show the $J-K$ and V-K colors as a function of K magnitude. Open circles denote stars without

TABLE 2. IR photometry for NGC 5927.

x (pixels)	y (pixels)	J (mag)	σ(J) (mag)	K (mag)	σ(K) (mag)	Optical ID		x (pixels)	y (pixels)	J (mag)	σ(J) (mag)	K (mag)	σ(K) (mag)	Optical ID	
345	123	14.40	0.08	13.52	0.01			524	124	12.15	0.08	10.93	0.01		
91	131	14.40		13.78				218	143	14.45	0.00	13.61	0.01	2	877
180	146	14.56	0.05	13.76	0.01	1	436	204	148	13.41	0.04	12.60	0.04	2	873
276	148	13.75	0.01	13.38	0.16	2	884	153	152	14.55	0.03	13.82	0.06	1	440
452	154	14.80	0.08	13.93	0.06			104	156	14.15		13.40	0.07	1	445
156	162	13.97	0.06	13.28	0.01	1	439	484	166	14.24	0.06	13.34	0.02		
111	169	14.21	0.00	13.53	0.11	1	447	264	171	14.09	0.03	13.32	0.01	2	888
113	177	13.70	0.01	12.96	0.06	1	448	265	177	14.82	0.01	13.99	0.10	2	889
312	177	11.47	0.05	10.42	0.03	2	886	106	179	14.64	0.10	13.84	0.04	1	449
335	183	14.02	0.02	13.25	0.03	3	907	159	185	14.03		13.39	0.02	1	463
174	193	14.61	0.06	13.85	0.01	1	464	127	194	13.78	0.01	12.97	0.00		
190	194	12.20	0.01	11.25	0.04			169	196	13.62	0.04	12.94	0.09		
184	199	14.34	0.02	13.57	0.02	1	467	192	206	13.57	0.01	12.86	0.01	1	468
390	210	14.28	0.03	13.66	0.16	3	904	106	214	14.18	0.01	13.52	0.03	1	459
129	213	13.99	0.01	13.35	0.05	1	476	288	213	13.14	0.06	12.57	0.05	2	892
142	215	14.54	0.10	13.86		1	474	460	216	10.83	0.01	10.11	0.00		
440	219	14.72	0.01	13.91	0.04	3	902	153	225	12.73	0.01	11.84	0.01	1	472
145	227	10.65	0.01	9.60	0.04	1	473	231	229	11.86	0.01	10.94	0.00	2	891
117	229	14.11	0.01	13.52		1	477	176	233	14.55	0.01	13.87	0.01	1	471
286	233	13.93	0.05	13.44	0.13	2	897	96	234	13.92	0.02	13.42	0.01	1	479
469	234	13.77	0.01	13.51	0.02			490	235	14.20	0.01	13.74	0.04		
526	235	12.61	0.03	11.90	0.05			374	236	11.76	0.04	10.89	0.05	3	1294
216	244	13.78	0.00	13.49	0.01	2	501	111	246	14.16	0.02	13.54	0.10	1	5
98	248	14.27	0.01	13.65	0.01	1	1	472	251	13.52	0.01	12.85	0.00		
186	252	14.11	0.01	13.42	0.04	1	10	517	252	14.86	0.07	13.86	0.02		
105	253	14.10	0.02	13.43	0.06	1	3	114	258	12.28	0.01	11.48	0.05	1	4
490	258	13.98	0.01	13.56	0.01			97	261	13.43	0.06	12.72	0.02	1	2
156	269	12.10	0.03	11.14	0.02	1	23	195	271	13.28	0.01	12.57	0.01	1	17
253	279	13.99	0.03	13.30	0.03	2	516	86	282	13.82		13.02	0.06		
393	285	14.56	0.04	13.71	0.03	3	1287	55	288	14.25	0.01	13.80	0.08		
216	289	13.52	0.09	12.79	0.04			109	289	12.33	0.03	11.45	0.01		
170	288	14.57	0.07	13.79	0.09	1	21	254	289	14.12	0.09	13.44	0.11	2	517
93	289	14.23	0.03	13.41	0.19			127	293	14.21	0.03	13.54	0.06	1	29
176	298	14.12	0.07	13.45	0.06	1	18	259	297	14.42	0.08	13.73	0.04	2	519
70	299	13.73	0.05	12.95	0.04			75	300	14.26	0.05	13.30	0.07		
96	301	13.79	0.07	13.15	0.08	1	33	206	301	13.91	0.05	13.26	0.10		
225	303	14.01	0.04	13.26	0.06	2	522	247	304	10.79	0.04	10.00	0.03	2	521
160	306	12.86	0.04	12.06	0.03	1	40	53	308	14.01	0.12	13.56	0.04		
66	308	14.23	0.05	13.40	0.01			167	308	13.90	0.03	13.21	0.08	1	41
469	308	12.86	0.03	11.95	0.01			193	311	14.02	0.03	13.25	0.07	1	44
247	304	13.94	0.08	13.24	0.05			243	311	14.72	0.14	13.98	0.13		
518	311	14.56	0.06	13.99	0.01			93	312	13.65	0.04	12.88	0.04		
248	312	13.86	0.05	13.60	0.30			92	316	13.70	0.08	13.04			
64	318	14.65	0.04	13.78	0.06			224	317	14.08	0.05	13.37	0.01	2	523
181	320	14.60	0.03	13.85	0.10	1	43	54	322	14.10	0.05	13.40	0.06		
435	322	13.19	0.01	12.36	0.01	3	1274	74	323	14.14	0.00	13.39	0.01		
153	325	12.71	0.02	11.88	0.00	1	38	61	328	14.27	0.01	13.65	0.07		
82	328	13.80	0.06	13.18				264	328	14.12	0.08	13.37	0.03	2	525
413	328	13.18	0.02	12.52	0.01	3	1276	256	329	14.08	0.06	13.28	0.09	2	524
348	330	14.50	0.10	13.86	0.01	3	1278	134	331	12.86	0.02	12.07	0.01	1	37
262	336	14.45	0.07	13.99	0.01	2	530	180	337	14.15	0.02	13.46	0.10	1	49
87	342	13.86	0.02	13.29	0.12	1	66	123	342	14.08	0.06	13.45	0.10	1	59
78	343	13.93	0.02	13.23	0.01	1	67	115	349	14.64	0.06	13.79	0.07	1	62
268	350	13.82	0.05	13.19	0.02	2	531	102	351	11.43	0.04	10.42	0.02	1	65

TABLE 2. (continued)

x (pixels)	y (pixels)	J (mag)	σ(J) (mag)	K (mag)	σ(K) (mag)	Optical ID		x (pixels)	y (pixels)	J (mag)	σ(J) (mag)	K (mag)	σ(K) (mag)	Optical ID	
73	352	13.47	0.06	12.68	0.00	1	68	57	354	14.04	0.04	13.64	0.01		
90	355	12.45	0.05	11.61	0.05	1	69	247	356	10.75	0.04	9.66	0.05	2	532
230	356	12.49	0.02	11.77	0.04	2	533	119	357	14.59	0.06	13.83	0.05	1	61
134	360	14.05	0.01	13.41	0.02	1	56	366	361	14.17	0.12	13.49	0.01	3	1269
324	363	12.99	0.04	12.12	0.04	3	1267	87	367	14.24	0.04	13.57	0.20	1	70
184	369	14.07	0.02	13.35	0.04	2	534	251	373	11.10	0.01	10.06	0.02		
218	374	11.80	0.03	10.86	0.02	2	536	344	376	14.67	0.18	13.93	0.09	3	1268
263	379	13.96	0.06	13.57	0.13	2	540	279	379	14.10	0.05	13.55	0.14	2	541
129	386	12.17	0.03	11.25	0.02			249	384	11.62	0.04	10.59		2	539
85	387	12.30	0.04	11.38	0.01	1	86	238	390	14.39	0.05	13.66	0.08	2	537
116	392	10.21	0.05	9.51	0.03	1	74	99	403	12.41	0.00	11.59	0.04	1	84
282	408	14.75	0.07	13.94	0.05	2	543	311	408	12.25	0.05	11.53	0.02	3	1265
164	410	13.84	0.09	13.04	0.07	2	549	108	415	12.77	0.01	12.00	0.04		
199	421	14.03	0.01	13.29	0.04	2	550	123	422	14.32	0.01	13.63	0.04	1	77
216	427	14.52	0.03	13.85	0.01	2	551	262	429	14.09	0.04	13.51	0.19	2	544
209	430	14.13	0.07	13.41	0.05			94	432	11.55	0.02	10.76	0.04	1	111
282	444	14.44	0.06	13.73	0.05			161	447	14.03	0.02	13.36	0.01	2	557
68	450	9.62		8.46		V	5	333	450	12.15	0.05	11.57		3	1254
122	452	14.01	0.02	13.32	0.04	2	559	325	456	11.63	0.03	10.99		3	1253
310	458	14.59	0.00	13.70		3	1252	309	465	14.09	0.11	13.34			
142	467	10.81	0.11	10.03	0.00			56	475	9.95		8.79		V	6
106	478	12.82	0.01	12.00	0.01	2	563	139	482	14.43	0.02	13.80	0.01		
259	483	14.12	0.01	13.37	0.03	3	1248	87	485	14.08	0.06	13.52		2	584
312	490	13.96	0.07	13.31		3	1244	265	500	14.01	0.06	13.38	0.05	3	1246
136	506	14.09	0.02	13.40	0.01	2	571	79	510	12.57	0.03	11.93	0.00	2	582
315	512	14.06	0.06	13.44		3	1242	215	515	13.80	0.00	13.03	0.04	3	1235
63	516	13.91	0.07	13.34	0.06	2	580	183	516	14.12	0.01	13.53	0.20	2	569
255	521	12.52	0.01	11.66	0.02	3	1238	126	533	13.52	0.01	12.95		2	573
171	541	13.33		12.66	0.04			203	549	14.41		13.79	0.07		
97	558	13.98		13.32	0.01			184	563	13.83		13.51	0.04		
72	570	12.68		11.93	0.03			90	580	14.66		13.85	0.00		
210	582	11.04		10.60	0.04										

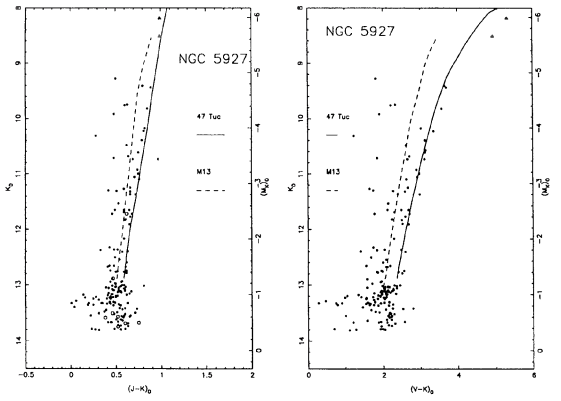

FIG. 1. (a) and (b) show the $J-K$ and V-K colors as a function of reddening-corrected K magnitude for the giants in NGC 5927. The open symbols in (a) denote stars for which no visual photometry is available. The two open triangles indicate two very red variables near the tip of the giant branch.

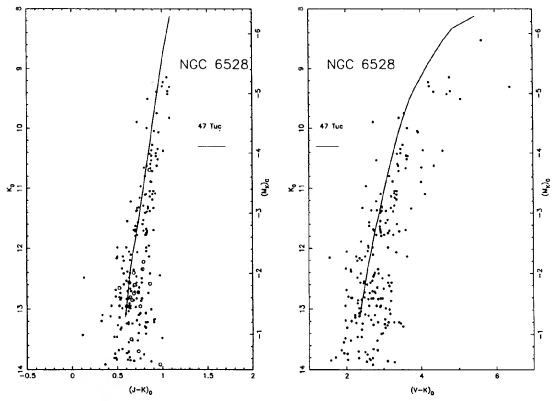

FIG. 2. The same as Figs. 1(a) and 1(b) for NGC 6528.

optical photometry, while filled circles denote those stars with optical photometry (the majority of the objects). In the infrared color–magnitude diagram, unlike in corresponding optical color–magnitude diagrams, the stars progress smoothly and monotonically brighter as they become redder. This phenomenon was discussed in Sec. *3.1*.

3.3 NGC 6624

NGC 6624 is a small globular cluster located close to the galactic center at a distance of 6.9 kpc. We have adopted $E(B-V)=0.28$ mag for this object. Photographic photometry is available from Liller & Carney (1978). Its metallicity is believed to be comparable to that of 47 Tuc, i.e., significantly less than that of NGC 5927 or NGC 6528. Three fields were observed on three different nights whose centers are $\approx$80 arcsec east, west, and south of the center of the globular cluster. Table 4 lists the measurements at J and at K for NGC 6624. The format is identical to Table 2. There is no previous infrared photometry for any stars in this globular cluster. The optical identifications are from Liller & Carney (1978). To supplement this rather old visual photometry, CCD frames were obtained through the V and R filters at the Yale 1.0 m telescope at CTIO in July 1993 using service observing. The data were reduced in standard ways (FIGARO and DAOPHOT) described above and the resulting magnitudes are listed in Table 5. The major purpose of the Tololo photometry was to obtain additional V magnitudes for stars observed in the infrared, but it also served to confirm the estimate of the magnitude level of the red horizontal branch, which is 15.98 $\pm$0.08 mag from the new data, and is given as 16.05 mag by Liller & Carney (1978).

Figures 3(a) and 3(b) show the $J-K$ and V-K colors as a function of K magnitude. Open circles denote stars without optical photometry, while filled circles denote those stars with optical photometry. There is some contamination by field stars, but the general morphology of the giant branch is obvious. The red horizontal branch appears at $V\approx16$ mag (Liller & Carney 1978), and is apparent in Fig. 3 as the group of stars with $K_0\approx13.2$ mag.

3.4 NGC 6171

NGC 6171 is a moderately metal poor globular cluster in the direction of the galactic center but at a galactic latitude of 23° with a fairly large reddening. We have adopted $E(B-V)=0.33$ mag. Optical photometry was given by Sandage & Katem (1964), while photometry reaching the main sequence was given by DaCosta *et al.* (1984). We covered several fields in the outer parts of the cluster from Las Campanas. Unfortunately, that night was not photometric, and the data were calibrated by repeating smaller fields in the outer parts of the cluster, and adding a field near the center with the infrared array on the 5 m Hale telescope at Palomar Mountain.

We use the numbering system of both Sandage & Katem (1964) (denoted "1") and that of DaCosta *et al.* (1984) (denoted "2"). Infrared magnitudes for the program stars are given in Table 6, while Figs. 4(a) and 4(b) show the $J-K$ and V-K colors as a function of K magnitude. The symbols are as before, with the addition of "*", which denotes an RR Lyrae variable, and of an open star, used for two stars which are definitely field stars based on their position in the V,

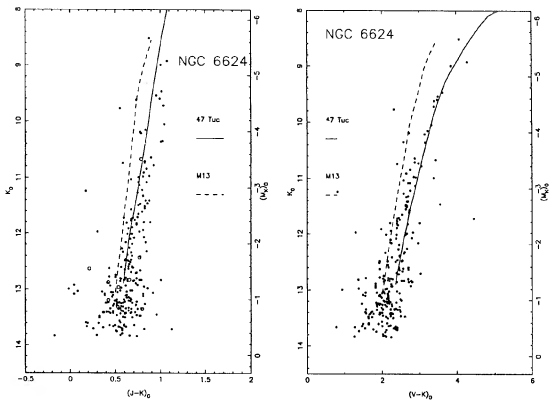

FIG. 3. The same as Figs. 1(a) and 1(b) for NGC 6624.

TABLE 3. IR photometry for NGC 6528.

x (pixels)	y (pixels)	J (mag)	σ(J) (mag)	K (mag)	σ(K) (mag)	V (mag)	Optical ID
181	96	12.61		13.96			
196	101	13.67	0.01	12.76	0.22	17.42	0 88
300	104	13.66	0.09	12.85	0.20		
358	107	12.98	0.01	11.99	0.07	16.47	0 99
253	111	12.97	0.01	12.18	0.21	16.32	2 44
154	114	12.64	0.00	11.74	0.04	16.20	0 115
318	111	12.26	0.01	11.09	0.08	16.64	0 107
277	117	14.81	0.00	13.92		17.39	0 119
191	120	13.27	0.01	12.26	0.11	17.14	0 127
182	122	10.83	0.03	9.70	0.03	16.30	0 130
384	123	14.19		13.15	0.25		
137	124	14.70	0.13	13.60		18.07	0 138
229	124	11.73	0.11	10.56	0.13	16.16	0 134
342	133	14.31		13.28		17.32	0 159
233	133	14.14	0.01	13.23		17.16	0 165
180	138	12.47	0.11	11.29	0.06	16.94	0 178
359	140	13.84	0.07	13.01	0.04	16.68	0 187
323	144	14.72	0.02	13.71		18.07	0 194
245	148	13.76	0.03	12.61		17.02	0 203
270	153	12.39	0.07	11.35	0.14	16.19	0 217
231	157	12.56	0.08	11.38		16.27	2 47
373	159	14.63	0.08	13.69	0.05		
209	163	12.21	0.02	11.16	0.02	15.24	0 239
237	169	12.72	0.07	11.57		16.18	2 49
364	174	12.80	0.03	11.72	0.07	16.37	0 273
249	176	12.43		11.24	0.07	16.14	2 50
384	182	13.90	0.18	12.64		17.32	0 295
114	184	13.75		12.69		17.20	0 300
149	196	11.95	0.02	10.71	0.06	15.88	2 39
140	199	14.80	0.06	13.89		17.75	0 356
351	202	14.67	0.15	13.87	0.11	17.27	0 362
387	206	13.81	0.04	12.81	0.03	17.50	0 377
340	209	13.93	0.13	13.03	0.07	17.16	0 391
375	220	14.02	0.08	13.02	0.14	17.48	0 433
217	221	11.31		10.19	0.06	15.37	1 5
379	226	14.38		13.43		18.42	0 450
216	228	14.31	0.12	13.29		17.06	0 461
251	99	13.91	0.07	13.29		17.59	0 80
309	102	13.07	0.00	12.18	0.05	16.43	0 89
211	107	14.75	0.04	14.00		18.24	0 98
199	110	13.62	0.01	12.73	0.18	16.97	0 102
309	110	14.25	0.03	13.46	0.23	18.09	0 103
265	112	13.89	0.01	12.91		17.21	0 109
324	113	13.10		12.68		14.54	0 112
334	117	14.32	0.05	13.41		18.07	0 120
247	120	14.02	0.01	13.10		16.94	0 129
304	122	14.69	0.28	13.85		18.11	0 135
122	124	13.92		13.02		17.23	0 137
204	124	12.90	0.12	11.91	0.11	16.87	0 139
256	131	14.06	0.01	12.93		17.25	0 156
384	133	13.94		12.92	0.18		
145	137	14.35	0.18	13.44	0.04	18.00	0 172
324	139	14.81	0.15	13.90		17.94	0 185
119	144	14.36		13.20		17.89	0 193
288	147	13.08	0.10	11.89		17.02	0 202
387	148	13.93		12.78	0.35		
281	154	13.87	0.06	12.84		17.21	0 219
244	157	13.02	0.06	11.90		16.60	2 48
174	160	12.84	0.01	11.83	0.08	16.27	2 41
321	168	11.83	0.04	10.61	0.03	15.61	2 7
343	170	13.24	0.08	12.30	0.05	16.56	2 54
103	175	13.47		12.33		17.50	0 276
361	182	13.60	0.04	12.54	0.03	16.93	0 294
106	184	11.94		10.85		16.41	0 301
336	191	12.05	0.07	10.82	0.08	16.71	0 322
333	198	13.07	0.10	11.97	0.07	16.77	0 349
345	201	11.95	0.09	10.79	0.07	15.71	2 8
327	204	12.66	0.09	11.53		16.81	2 55
132	207	14.07	0.00	13.14	0.06	17.29	0 386
378	214	14.51	0.11	13.41		18.22	0 408
135	220	14.35	0.07	13.53		17.48	0 435
338	223	11.77	0.11	10.62	0.08	15.53	2 9
142	228	14.02		13.18		17.06	0 456
372	228	13.81	0.10	13.00	0.09	17.03	0 462

TABLE 3. (continued)

x (pixels)	y (pixels)	J (mag)	σ(J) (mag)	K (mag)	σ(K) (mag)	V (mag)	Optical ID	x (pixels)	y (pixels)	J (mag)	σ(J) (mag)	K (mag)	σ(K) (mag)	V (mag)	Optical ID
137	230	13.86		13.14		16.65	2 37	381	231	14.57	0.09	13.48		18.53	0 471
226	232	13.86	0.09	13.04	0.22	16.99	0 476	325	233	12.56	0.07	11.48		16.31	2 58
105	234	13.95		13.14		17.60	0 486	221	235	13.35	0.05	12.24	0.13	16.36	0 502
237	235	13.14	0.04	12.36	0.13	16.26	0 496	214	237	12.81	0.01	11.82	0.13	15.98	0 503
229	237	12.86	0.05	11.89	0.09	16.20	0 505	233	239	12.70	0.12	11.58	0.17	16.38	0 516
210	240	13.12	0.11	12.33	0.15	16.38	0 518	251	240	11.10	0.05	10.09	0.08	14.36	0 520
353	239	13.70	0.07	12.77	0.06	16.78	0 517	345	243	12.39	0.09	11.24	0.07	16.08	2 62
241	244	10.97	0.06	9.62	0.06	15.86	0 537	371	244	14.65	0.06	13.74	0.13	17.20	0 531
199	246	13.66	0.10	12.74	0.28	16.76	0 542	113	248	12.35		11.41		15.76	0 548
212	246	11.94	0.10	10.82	0.08	15.76	0 544	351	247	12.53	0.08	11.52	0.08	15.50	2 10
338	251	13.76	0.14	12.76		16.95	0 559	116	253	14.11		13.06		17.79	0 569
165	253	10.92	0.04	9.57	0.02	15.90	1 27	200	250	13.47	0.10	12.61	0.17	16.54	0 560
217	250	11.44	0.16	10.24	0.12	15.69	0 561	243	250	12.40	0.07	11.30	0.10	16.19	0 564
226	252	12.57	0.03	11.57	0.06	16.06	0 567	136	252	12.86	0.04	11.79	0.02	16.69	0 570
367	255	13.57	0.07	12.60	0.06			109	256	13.79		12.86		17.40	0 579
207	257	10.81	0.11	9.58	0.13	15.47	0 588	212	259	10.78	0.16	9.49	0.09	15.26	0 589
228	259	12.02	0.13	10.86		16.00	0 595	225	260	12.09	0.07	10.99	0.11	15.69	0 604
374	257	14.05	0.11	13.14	0.16	17.49	0 587	360	261	14.14	0.06	13.33	0.06	17.10	0 609
365	262	14.40	0.12	13.65	0.06	17.59	0 614	134	262	14.32	0.11	13.43		17.40	0 616
206	264	10.72	0.08	9.42		15.17	0 618	216	265	12.57	0.07	11.56	0.08	15.93	0 625
223	265	13.26	0.13	12.40	0.14	16.24	0 627	343	265	14.66	0.21	13.71	0.08	17.36	0 620
113	268	13.84		12.90		17.64	0 636	371	268	14.91	0.21	13.89	0.10		
243	269	11.82	0.07	10.65	0.07	15.80	0 646	387	270	12.98		11.97	0.08	16.32	0 638
179	272	12.49		11.28		16.11	1 25	107	274	13.79		12.82		17.52	0 659
235	277	12.54	0.04	11.51		16.01	0 673	136	278	14.00	0.07	13.39	0.25	17.06	0 680
388	278	14.02		13.31	0.16	17.19	0 677	230	279	11.65	0.06	10.47	0.06	15.53	0 688
338	281	14.02		13.62		15.51	2 11	378	282	13.82	0.18	12.76	0.11	17.51	0 701
129	283	13.53	0.04	12.60	0.09	16.91	0 708	121	287	14.08		13.02		17.53	0 720
113	290	13.92		13.03		17.42	0 731	355	290	14.69	0.13	13.93	0.06	17.49	0 735
374	292	13.65	0.09	12.79	0.12	16.89	0 740	128	293	14.43	0.06	13.65	0.02	17.48	0 747
145	294	13.18		12.33		16.14	2 4	173	294	11.51	0.05	10.26	0.06	15.73	1 2
149	302	13.75	0.03	12.93	0.04	17.10	0 783	118	306	14.10		13.18		17.77	0 791
260	308	11.78	0.16	10.54	0.06	15.54	0 27	327	308	12.57	0.06	11.56	0.04	15.78	2 12
284	309	11.87	0.03	10.57	0.06	16.69	0 809	118	310	14.15		13.27		17.98	0 811
183	317	13.60		12.68		16.52	2 32	375	318	14.00	0.08	13.05			
333	319	12.09	0.01	10.91	0.03	15.86	2 69	175	322	12.98		11.87		16.32	2 33
361	330	13.08	0.04	11.97	0.06	16.53	0 881	333	333	11.88	0.08	10.66	0.07	15.85	2 70
356	333	14.48	0.06	13.45		17.71	0 896	194	340	13.14		12.35		15.44	2 17
251	340	12.63		11.50	0.05	16.00	2 22	387	340	12.87	0.04	11.88	0.07	16.15	0 919
367	341	13.05	0.09	11.94	0.20	16.60	0 930	152	344	13.48	0.00	12.58		16.25	2 34
381	349	11.39	0.09	10.02		14.98	0 951	182	353	12.24		11.08		15.87	2 3
210	353	12.98		11.90		16.36	2 24	357	353	13.65	0.13	12.88	0.05	16.42	0 964

TABLE 3. (continued)

x (pixels)	y (pixels)	J (mag)	σ(J) (mag)	K (mag)	σ(K) (mag)	V (mag)	Optical ID	x (pixels)	y (pixels)	J (mag)	σ(J) (mag)	K (mag)	σ(K) (mag)	V (mag)	Optical ID
353	355	13.37	0.08	12.53	0.09	16.06	0 968	140	356	14.56	0.11	13.37		17.57	0 973
314	356	13.29	0.11	12.18	0.13	16.84	0 975	339	356	14.30		13.26	0.02	17.14	0 972
237	359	15.02		13.94		18.04	0 981	298	359	12.48	0.09	11.33	0.09	16.08	2 19
182	360	13.52	0.12	12.55		16.21	2 2	330	360	13.17	0.07	12.25	0.06	15.80	0 988
374	361	14.91	0.07	13.99	0.21	17.23	0 989	392	361	13.94		12.92		16.95	0 987
136	365	14.33	0.32	13.50	0.22	17.05	01001	221	365	13.66	0.12	12.66	0.11	16.93	01003
268	369	13.78	0.12	12.80	0.06			293	370	13.76	0.07	12.99	0.08	16.58	2 18
226	372	16.12		12.48	0.04			353	372	15.85		12.48			
232	376	14.02	0.18	13.05	0.00	16.90	2 26	144	378	14.36	0.09	13.26	0.02	17.16	01048
355	379	11.90	0.04	10.73	0.09	15.09	01054	327	380	13.93	0.00	13.01		16.70	01058
374	379	13.02	0.06	11.90	0.03	16.19	01056	157	381	14.56		13.36	0.04	17.93	01059
176	387	13.29	0.03	12.15		16.28	01082	293	387	14.60	0.09	13.41		17.79	01083
204	388	14.04	0.08	13.15	0.17			281	393	13.91	0.14	12.94	0.21		
211	390	13.32	0.04	12.39	0.08	16.35	01096	207	391	14.15	0.11	13.16		17.60	01100
198	395	13.69	0.07	12.76	0.12	16.68	01109	244	395	12.71	0.02	11.52	0.12	16.26	01111
284	396	14.11	0.20	13.18	0.27	17.11	01114	294	396	14.60	0.23	13.50	0.22	18.08	01112
227	396	13.05	0.02	11.93	0.06	16.40	01116	172	397	10.68	0.06	9.34		15.65	01113
187	399	13.80	0.17	12.90	0.23	17.14	01122	214	400	14.38		13.38	0.31	16.89	01120
222	401	12.40	0.02	11.29	0.07	15.76	01128	157	402	12.04	0.09	10.89	0.06		
308	402	11.17	0.04	9.94	0.04	15.04	01134	201	404	12.70	0.03	11.60	0.04	16.06	01139
129	405	14.95		13.67		17.17	01137	161	406	13.93	0.01	13.00			
193	407	10.87	0.03	9.50		17.43	01141	223	407	13.50	0.08	12.42	0.02		
245	408	12.78	0.04	11.76	0.08	15.92	01147	174	410	14.61	0.01	13.59	0.01	18.10	01156
305	410	14.53	0.02	13.41		18.35	01155	241	411	13.61	0.11	12.54			
333	416	14.77		14.00		17.87	01170								

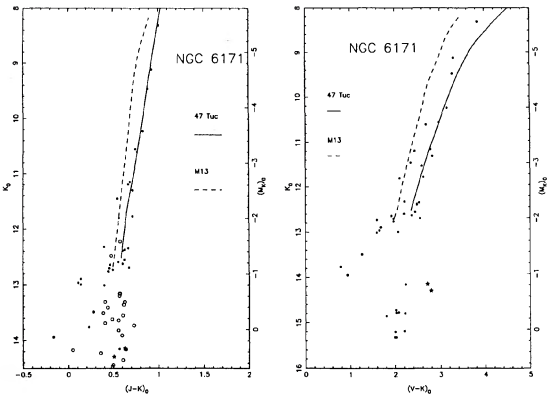

FIG. 4. The same as Figs. 1(a) and 1(b) for NGC 6171. Two definite field stars are plotted with open asterisks, while a filled "*" indicates the single RR Lyrae variable we observed in this cluster.

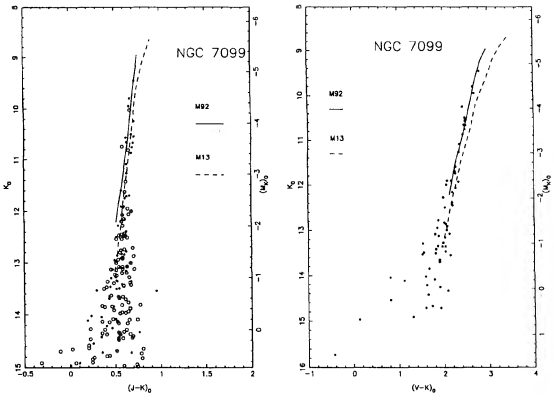

FIG. 5. The same as Figs. 1(a) and 1(b) for NGC 7099. A filled "*" denotes the single RR Lyrae variable we observed in this cluster.

$B-V$ diagram of DaCosta *et al.* (1984), and verified by their position in Fig. 4. There are three stars in common with the earlier photometry of Frogel *et al.* (1983b). They are the three brightest stars observed here. We obtain for them $\Delta(K)=0.03$ mag and $\Delta(J-K)=0.05$ mag with a dispersion of less than 0.01 mag in both cases. The older measurements are somewhat brighter in both J and K.

The presence of RR Lyrae variables offers us a chance to determine the distance modulus in a manner which is much more independent of reddening than the usual optical procedures. We use the infrared period–luminosity relationship established by the work of many people for field RR Lyrae stars and summarized by Jones *et al.* (1992). Using the periods derived from optical photometry in the catalog of Sawyer Hogg (1973), we determine a distance of 5.2 ± 0.4 kpc. The distance modulus derived from the mean apparent visual magnitude of the horizontal branch which we adopt here is 5.8 kpc, in reasonable agreement with that value. Note that the optical distance modulus is critically dependent on the choice of reddening. Additional infrared photometry of RR Lyrae variables in globular clusters should prove very informative.

3.5 NGC 7099

NGC 7099 is a low metallicity globular cluster at high galactic latitude with low reddening at a distance of 7.4 kpc. We have adopted $E(B-V)=0.05$ mag. Optical photometry was given by Dickens (1972), while Alcaino & Liller (1980) give deeper photographic photometry reaching the main sequence. We have also taken a few V magnitudes from the shortest exposure field studied by Bolte (1987). In addition, to reach the brightest stars, most of which have no published visual photometry, we took two 20 s exposures with the 1.5 m telescope at Palomar Mountain, and used the published Dickens photometry to calibrate our DAOPHOT measurements. The major peculiarity of NGC 7099 discerned from these studies is a relative paucity of red giants compared to horizontal branch stars. One speculative explanation advanced by Dickens is that the He abundance in NGC 7099 is unusually high. We cover three fields on four nights with the infrared array. The first is centered about 1 arcmin north of the cluster center, the second 1 arcmin directly south of the center, and the third is 1 arcmin east of the second field. The scarcity of red giants is apparent from these images. We can resolve stars essentially into the center of the cluster, but the region with a radius of 10 arcsec of the cluster core was eliminated, as the photometry showed a large scatter.

All of the nights on which this cluster was observed from Las Campanas were not photometric. So the images were calibrated by frames taken with the infrared array camera on the 5 m Hale telescope at Palomar Mountain. This cluster is rather far south to be observed from Palomar with high precision (the airmass always exceeds 1.8), and hence there is a 0.04 mag uncertainty in the zero point of the $J-K$ colors. The infrared photometry is given in Table 7; magnitudes given in parenthesis under the column for the optical identification are our new Palomar measurements. Figures 5(a) and 5(b) present the infrared color–magnitude diagrams with the usual meaning of the symbols.

We use the numbering system of Dickens as it covers the spatial and magnitude range spanned by our data better than does the later work. Note that because of the sparseness of the field and the absence of a sheet of field stars, as well as the better seeing, we are able to reach to $K\approx16$ mag, albeit with significant measurement errors. We clearly see the previously known horizontal branch stars in our fields. There are only three RR Lyrae variables known in this cluster (Sawyer Hogg 1973), and one of these falls within the area we studied. For this single variable, imaged at K at a random single phase, and using the infrared period–luminosity law described in the references in Sec. *3.4* on NGC 6171, we obtain a distance modulus within 0.1 mag of that adopted here.

4. RESULTS

We discuss two major properties of our data. First we consider the spread in the giant branches of the five globular clusters for various colors, and try to distinguish between the various possible causes of it. We then examine the reddening

TABLE 4. IR photometry for NGC 6624.

x (pixels)	y (pixels)	J (mag)	σ(J) (mag)	K (mag)	σ(K) (mag)	Optical ID		x (pixels)	y (pixels)	J (mag)	σ(J) (mag)	K (mag)	σ(K) (mag)	Optical ID	
391	-32	12.03	0.13	11.08	0.02			481	-9	14.20	0.15	13.32	0.01		
471	14	14.25	0.07	13.38				345	24	14.37		13.51			
436	32	13.36	0.06	12.58	0.21			385	39	14.43		13.60	0.12	2	153
550	44	13.13	0.09	12.17	0.09			343	50	14.03	0.05	13.24	0.00	2	142
348	54	14.10	0.06	13.28	0.00	2	143	392	56	14.14		13.52		2	151
312	59	13.62	0.05	13.03				333	61	14.07	0.07	13.32		2	141
381	72	13.62	0.26	12.91				330	74	14.47	0.08	13.73		2	139
526	74	14.05		13.50	0.04	3	111	413	75	13.52	0.04	12.73	0.07	2	155
452	79	14.02	0.03	13.36	0.12	3	106	459	79	14.34	0.01	13.45		3	107
316	82	13.16	0.10	12.36				487	84	14.17	0.06	13.22		3	109
343	87	14.44	0.08	13.56		2	144	307	89	13.77		13.15		2	137
378	94	12.62	0.03	11.65	0.12			312	95	13.71	0.06	13.18		2	136
285	104	14.39		13.45				345	108	14.20	0.12	13.44	0.12	2	145
324	111	13.79	0.10	12.95	0.10	2	135	250	112	14.27	0.02	13.48	0.06	2	123
294	113	13.86	0.07	12.93	0.01	2	131	549	116	13.86	0.11	12.99		3	117
409	116	14.22	0.20	13.16	0.10	2	51	297	118	13.79	0.07	13.03	0.07	2	130
283	123	14.07	0.04	13.34		2	126	420	124	13.68	0.01	12.76	0.13	2	51
592	127	13.09		12.73				379	129	14.02	0.03	13.25	0.12	2	45
453	129	11.95	0.03	10.88	0.05	3	7	475	131	13.53		12.70		3	11
478	131	13.52	0.06	12.69		3	11	363	134	12.65	0.03	11.71	0.10	2	43
388	138	13.97	0.10	13.20	0.21	2	46	350	140	12.08	0.04	11.18	0.09	2	36
504	142	12.38	0.08	11.43	0.08	3	12	537	142	14.14	0.13	13.44	0.07	3	124
401	143	13.94	0.11	13.30	0.16	2	48	122	145	13.68	0.10	12.80	0.05		
561	145	13.94	0.16	13.28	0.01	3	126	548	147	11.21	0.10	10.29	0.06	3	125
575	151	14.02	0.12	13.33	0.01			438	152	12.72	0.03	11.86	0.06	3	5
457	153	14.08	0.09	12.93		3	8	460	153	14.02	0.01	13.28		3	8
229	154	14.01	0.06	13.39	0.06	2	119	322	157	14.82		13.94		2	35
466	160	14.13		13.18				469	161	13.73		12.93			
447	162	13.41	0.05	12.42	0.14	3	4	473	162	13.74	0.21	13.06			
656	162	10.57	0.01	9.87	0.01			389	168	13.70	0.10	12.92	0.10	2	41
321	175	13.75	0.12	13.15	0.28	2	28	118	176	13.45	0.08	12.87	0.03		
598	178	14.01		13.69	0.28	3	129	274	179	14.27	0.07	13.52	0.04		
324	181	14.06	0.02	13.35	0.15	2	29	243	183	14.03	0.06	13.51	0.02	2	115
291	183	14.09	0.11	13.30	0.02	2	117	337	188	13.68	0.06	12.81	0.01	2	31
409	193	10.24	0.01	9.02	0.07			534	193	14.33	0.08	13.52	0.01	3	21
438	194	10.73	0.02	9.57	0.18	3	2	502	196	14.02	0.11	13.51			
378	199	13.65	0.11	12.89	0.01	2	40	430	201	14.49	0.04	13.57			
192	202	13.78	0.06	13.07	0.05			533	203	13.26	0.08	12.44	0.01	3	22
432	205	14.16		13.70				439	208	14.11	0.04	13.49			
546	208	14.13	0.12	13.45		3	23	318	213	13.99	0.04	13.36	0.01	2	21
535	214	11.23	0.06	10.25	0.05			538	215	11.34	0.01	10.15			
434	216	12.49		11.57				503	216	14.27	0.18	13.45		3	19
238	217	12.37	0.06	11.42	0.03	2	111	437	217	12.53	0.02	11.51			
665	218	14.61		13.89	0.00			379	219	13.03	0.10	12.18	0.04		
429	219	13.38	0.04	12.59	0.08			338	220	13.93	0.05	13.12	0.01	2	25
413	220	13.01	0.04	12.20				589	220	13.33	0.03	12.58	0.03	3	132
310	221	14.59	0.04	13.74	0.05	2	20	331	223	13.61	0.04	12.79	0.02	2	22
269	225	14.62	0.03	13.92	0.03	2	18	376	224	13.45	0.11	12.65	0.03		
256	225	13.39	0.04	12.57	0.01	2	110	513	225	14.02	0.23	13.34	0.24	3	20
656	226	11.66	0.04	11.34	0.02			596	227	14.32		13.59	0.13	3	133
340	229	14.23	0.05	13.53	0.01	2	24	382	230	13.64	0.21	13.14	0.10		
332	234	14.28	0.06	13.52	0.01	2	14	370	233	10.84	0.06	9.70	0.10		
519	234	12.49	0.13	11.59	0.03	3	27	326	236	13.78	0.03	12.90	0.02	2	13
444	238	12.93		12.11				320	239	13.53	0.02	12.88	0.13	2	12

TABLE 4. (continued)

x (pixels)	y (pixels)	J (mag)	σ(J) (mag)	K (mag)	σ(K) (mag)	Optical ID		x (pixels)	y (pixels)	J (mag)	σ(J) (mag)	K (mag)	σ(K) (mag)	Optical ID	
217	241	14.33		13.51	0.02			424	241	13.54	0.03	12.97	0.04		
715	241	13.49		12.74	0.01			205	242	14.14		13.41	0.00	2	102
382	246	10.74	0.07	9.64	0.11			390	244	13.22	0.12	13.09			
147	245	13.65	0.09	12.95				398	246	13.86	0.10	13.29			
559	247	12.86	0.11	11.90	0.02	3	35	655	247	12.56		11.82	0.03	3	139
227	248	13.73	0.02	12.95	0.06	2	104	323	249	12.26	0.03	11.37	0.01	2	11
371	249	14.65		13.55				333	252	13.97	0.01	13.21			
567	252	12.66		11.84	0.03			414	253	13.44	0.06	12.53	0.19		
332	255	13.67	0.03	12.93	0.04			373	255	14.38		13.74	0.13		
434	255	9.63		8.61				310	256	13.33	0.03	12.50	0.03	2	7
348	256	11.61	0.13	10.46	0.07			404	255	14.01	0.07	13.05			
420	256	12.80	0.08	12.01	0.10			333	259	13.98	0.01	13.32	0.02		
402	260	12.99	0.07	12.04	0.00			570	260	13.91	0.08	13.02		3	36
411	261	13.79	0.03	12.94	0.04			425	261	13.16	0.06	12.43			
457	261	11.00	0.04	9.82				472	261	14.37		13.44			
527	261	13.36	0.28	13.13	0.13	3	30	716	263	13.32		12.56	0.02		
382	264	14.04	0.14	13.70				396	264	12.82	0.07	11.94	0.05		
330	265	14.17	0.18	13.34	0.06	2	6	487	265	12.82	0.05	11.99			
401	266	13.42	0.08	12.61	0.14			428	266	12.17	0.07	11.18			
616	266	11.99		11.09	0.05			706	266	14.53		13.77			
263	268	12.80	0.05	11.92	0.01			645	268	13.88		13.34	0.02	3	142
467	270	10.60		9.72				358	271	13.36	0.06	12.58	0.08		
531	271	11.57	0.03	10.84	0.02			411	272	13.44		12.53	0.01		
561	272	13.82		13.12	0.02	3	39	342	273	12.65	0.03	11.75	0.00		
387	273	13.48	0.01	12.69	0.09			400	272	14.08		13.08			
415	275	11.70		10.77	0.05			546	275	14.07		13.26	0.01	3	34
335	277	14.08	0.03	13.41	0.06			668	278	14.07		13.50	0.04	3	141
319	279	14.12	0.01	13.31	0.08			539	280	12.68		11.91	0.02		
552	280	12.14	0.03	11.23	0.02	3	40	260	281	12.56	0.04	11.56	0.02	2	1
382	281	14.22		13.49	0.16			373	283	11.97	0.01	11.01	0.01		
392	283	10.24		9.09				403	284	12.58	0.01	11.61			
619	284	13.82		13.15	0.02	3	150	323	285	11.93	0.11	10.94	0.01		
562	285	14.49		13.75		4	1	189	286	13.21	0.06	13.02	0.10	1	153
553	286	13.24	0.11	12.26	0.04			334	287	14.19	0.06	13.48			
611	287	13.89		13.34	0.01	4	101	398	288	13.65		12.89			
410	288	13.37		13.18				369	288	13.43	0.07	12.51	0.05		
420	288	11.62		10.45	0.04			709	291	11.24		10.31	0.02		
231	292	14.22	0.00	13.56	0.01	1	152	281	292	14.77	0.13	13.81	0.06	1	42
288	292	13.67		12.92		1	43	387	293	14.29	0.01	13.78	0.11		
762	295	13.99		13.36				232	297	14.03	0.04	13.44	0.00	1	151
515	297	14.20		13.80	0.04			412	299	14.38		13.76			
399	302	11.78	0.04	10.74	0.03			298	300	14.05	0.04	13.39		1	44
388	301	14.55	0.01	13.83				693	303	12.52	0.04	12.07	0.01		
763	304	11.95		11.13				375	305	13.91	0.02	13.14	0.13		
418	307	12.93		11.90	0.03			155	310	12.98	0.01	12.07	0.03		
293	311	14.09	0.06	13.76	0.07	1	39	606	311	14.45		13.77	0.00	4	104
639	311	13.90		13.33	0.04	4	103	410	312	12.94		12.11	0.03		
319	315	15.08		13.81				673	317	13.84		13.23	0.01		
557	322	14.22		13.43	0.04	4	9	601	324	14.52		13.80	0.01	4	105
353	326	12.09	0.03	11.07	0.01			320	326	14.03	0.01	13.34		1	31
372	328	14.33	0.16	13.36				534	329	14.32		13.74	0.02		
736	330	14.49		13.84	0.01			309	331	12.66	0.04	11.82	0.04	1	32
291	332	13.02	0.04	12.26		1	34	498	332	13.90		13.93			
506	332	14.07		13.60				565	332	12.89		12.11	0.04	4	10
385	333	12.49	0.02	11.51	0.01			325	333	14.73	0.01	13.93		1	30
624	333	14.11		13.40	0.02	4	106	253	336	12.69	0.04	11.87	0.04	1	141

TABLE 4. (continued)

x (pixels)	y (pixels)	J (mag)	σ(J) (mag)	K (mag)	σ(K) (mag)	Optical ID		x (pixels)	y (pixels)	J (mag)	σ(J) (mag)	K (mag)	σ(K) (mag)	Optical ID	
670	336	13.60		12.90	0.01			299	337	12.26	0.04	11.32	0.01	1	33
587	342	12.49		11.67	0.02	4	112	762	343	14.05		13.58			
406	349	11.78	0.02	10.81	0.04			555	350	13.49		12.84	0.01	4	12
395	355	13.26	0.03	12.48				385	364	13.54	0.10	12.98	0.01		
542	366	11.80		10.83	0.02	4	21	532	367	13.82		13.12	0.01	4	20
574	367	14.36		13.92	0.07	4	119	378	368	13.12	0.08	12.29	0.03		
129	369	13.73		13.20	0.06			570	370	13.09		12.37	0.03	4	120
299	376	14.51		13.85		1	20	235	378	14.48	0.03	13.57	0.07	1	137
566	378	14.48		13.78	0.03	4	121	635	378	13.30		12.72	0.01	4	111
215	381	13.84	0.01	12.93	0.07	1	135	689	381	14.11		13.52	0.02		
668	383	13.41		12.70	0.03			655	387	14.39		13.69			
353	388	12.49	0.08	11.59	0.01			387	390	13.95	0.08	13.12			
588	397	13.82		13.20	0.06			736	399	14.35		13.66	0.02		
561	406	12.70		11.81	0.07			755	416	14.28		13.53	0.08		
629	417	14.35		13.60	0.18			723	420	13.55		12.71	0.04		

corrected colors of the mean giant branch of each cluster at a fixed luminosity and use those parameters to study the metallicity of this sample of globular clusters.

4.1 The Widths of the Giant Branches

An interesting point to note is the relatively large spread in color at a given magnitude seen in the $K,(V-K)$ color–magnitude diagrams. This spread in $V-K$ within a globular cluster along the giant branch is sometimes quite large, reaching 0.6 mag for NGC 6528. The spread within a given cluster in $J-K$ is smaller, as is the spread in $B-V$. These spreads can arise either from patchy interstellar reddening or from metallicity variations among the stars in a particular globular cluster. The measurements of parameters describing these spreads are given for two luminosities at K_0, -3 and -4 mag in Table 8. In general, the color spread measurements are more reliable at the higher luminosity, where the uncertainties in the infrared photometry of any individual star are small and do not contribute. Note that the widths given are full widths of the color distribution, not σ values. The values of $\delta(B-V)$ were measured from the color–magnitude diagrams in the references for the optical photometry given in Sec. 3.

We rule out the effect of a strong AGB or of the presence of field stars. Even a strong AGB can only produce a range in colors which is small compared to that under discussion here. Also, the AGB component will appear as a distinct feature blueward of the first ascent red giants, especially at low luminosities, rather than as a complete blurring out of the giant branch in color. Note that the observed spreads are seen all along the giant branch independent of luminosity (until the luminosity is so low that the infrared magnitudes measured with a 1 m telescope become very imprecise). Some field star contamination of our sample has undoubtedly occurred, and we have ignored all stars bluer than the M13 locus in NGC 5927 and in NGC 6624. Background frames taken 10 arcmin away from the cluster field for each of the five clusters show that it is in general minimal and not important here.

We can use the ratio of width of the giant branch at a fixed M_{K_0} in various colors, particularly when the spreads are large, to try to differentiate between the effects of patchy interstellar reddening and those of a real metallicity spread within these metal rich clusters. Recall that there is essentially no data on the possible presence of a metallicity range within the very metal rich galactic globular clusters. Furthermore, spectroscopic studies of sufficient accuracy to detect small abundance variations within a globular cluster are of necessity confined to small samples of stars. Unless very large samples are examined spectroscopically, this issue cannot be probed, as any specific star which shows an abnormality could always be dismissed as a field star.

The dependence of the predicted width of the giant branch in various colors if patchy reddening occurs is deduced from the wavelength dependence of the interstellar reddening law. The dependence of the giant branch location for various infrared colors on metallicity is taken from Eq. (7) of Frogel *et al.* (1983a). Table 9 compares the ratios of the color

TABLE 5. *V* and *R* photometry for NGC 6624.

x (pixels)	y (pixels)	Star ID	V(CTIO) (mag)	Δ (V) (mag)	V−R (mag)	x (pixels)	y (pixels)	Star ID	V(CTIO) (mag)	Δ (V) (mag)	V−R (mag)
391	-32		14.77		0.89	481	-9		16.48		0.69
471	14		16.43		0.68	345	24		16.51		0.70
436	32		15.51		0.73	385	39	2- 153	16.61	0.06	0.73
550	44		15.75		0.82	343	50	2- 142	16.12	0.07	0.66
348	54	2- 143	16.45	0.13	0.72	392	56	2- 151	16.14	0.10	0.71
312	59		16.06		0.75	333	61	2- 141	16.18	0.07	0.66
381	72		15.06		0.55	330	74	2- 139	16.61	0.12	0.70
526	74	3- 111	16.19	0.09	0.64	413	75	2- 155	16.14	0.08	0.86
452	79	3- 106	16.10	0.05	0.60	459	79	3- 107	16.61	0.09	0.71
316	82		15.81		0.83	487	84	3- 109	16.10	0.06	0.62
343	87	2- 144	16.75	0.09	0.70	378	94		15.07		0.75
345	108	2- 145	16.36	0.09	0.68	324	111	2- 135	16.43	0.11	0.84
250	112	2- 123	16.65	0.10	0.81	294	113	2- 131	16.18	0.12	0.80
549	116	3- 117	15.90	0.12	0.63	409	116	2- 51	16.73	-0.64	0.76
297	118	2- 130	15.93	0.16	0.68	283	123	2- 126	16.21	0.10	0.67
420	124	2- 51	16.02	0.07	0.75	379	129	2- 45	16.02	0.14	0.62
453	129	3- 7	14.73	-0.01	0.87	475	131	3- 11	16.05	0.13	0.80
478	131	3- 11	16.05	0.13	0.80	363	134	2- 43	15.21	0.01	0.82
388	138	2- 46	16.06	0.09	0.65	350	140	2- 36	14.70	0.01	0.83
504	142	3- 12	14.91	-0.05	0.77	537	142	3- 124	16.45	0.10	0.66
401	143	2- 48	16.06	0.14	0.61	122	145		16.61		0.92
561	145	3- 126	16.03	0.07	0.59	548	147	3- 125	13.77	0.03	0.78
575	151		16.25		0.63	438	152	3- 5	15.10	-0.06	0.73
457	153	3- 8	16.27	-0.03	0.71	460	153	3- 8	16.27	-0.03	0.71
229	154	2- 119	16.14	0.15	0.66	466	160		16.12		0.65
447	162	3- 4	15.74	0.07	0.72	656	162		12.98		0.71
389	168	2- 41	15.72	0.06	0.64	321	175	2- 28	15.84	0.09	0.68
118	176		15.59		0.63	598	178	3- 129	16.01	0.10	0.59
274	179		16.51		0.66	324	181	2- 29	16.29	0.10	0.69
243	183	2- 115	15.76	0.10	0.56	291	183	2- 117	16.01	0.13	0.61
337	188	2- 31	15.92	0.12	0.72	409	193		14.09		1.12
534	193	3- 21	16.50	0.09	0.66	438	194	3- 2	13.93	0.05	0.99
502	196		15.98		0.58	378	199	2- 40	15.65	0.05	0.66
430	201		16.45		0.68	192	202		15.98		0.72
533	203	3- 22	15.69	0.12	0.71	432	205		16.38		0.67
439	208		15.98		0.60	546	208	3- 23	16.59	0.06	0.66
318	213	2- 21	15.92	0.08	0.61	535	214		14.26		0.91
538	215		14.26		0.91	434	216		14.99		0.77
503	216	3- 19	16.01	0.08	0.59	238	217	2- 111	14.93	-0.03	0.83
437	217		14.99		0.77	665	218		16.69		0.62
379	219		15.34		0.73	429	219		15.74		0.73
338	220	2- 25	16.01	0.08	0.67	413	220		15.21		0.69
589	220	3- 132	15.77	0.12	0.69	310	221	2- 20	16.67	0.02	0.70
331	223	2- 22	15.84	0.12	0.70	269	225	2- 18	16.78	0.00	0.68
376	224		15.59		0.70	256	225	2- 110	15.79	0.11	0.75
513	225	3- 20	15.96	0.07	0.61	656	226		12.94		0.36
596	227	3- 133	16.56	0.11	0.64	340	229	2- 24	15.94	0.03	0.58
382	230		15.48		0.59	332	234	2- 14	16.51	0.05	0.69
370	233		13.97		0.99	519	234	3- 27	15.09	-0.08	0.77
326	236	2- 13	16.27	0.11	0.74	444	238		15.28		0.86
320	239	2- 12	15.74	0.09	0.68	217	241		16.55		0.71
715	241		16.00		0.73	205	242	2- 102	16.03	0.14	0.58
382	246		13.93		0.99	390	244		14.81		0.50
147	245		16.45		0.86	559	247	3- 35	15.57	0.12	0.82
655	247	3- 139	15.01	0.00	0.69	227	248	2- 104	16.01	0.12	0.71
323	249	2- 11	14.80	-0.07	0.78	371	249		16.35		0.65
333	252		15.95		0.61	567	252		15.10		0.72
332	255		15.91		0.63	373	255		15.98		0.58
434	255		13.47		1.18	310	256	2- 7	15.67	0.09	0.73
348	256		14.40		0.92	404	255		15.66		0.51
420	256		14.77		0.67	333	259		15.94		0.60
402	260		15.06		0.65	570	260	3- 36	16.49	0.08	0.80
411	261		15.77		0.67	425	261		15.30		0.60
457	261		14.00		0.94	472	261		15.79		0.59
527	261	3- 30	15.86	0.07	0.62	716	263		15.76		0.69
382	264		15.97		0.59	396	264		15.15		0.72
330	265	2- 6	15.96	0.02	0.62	487	265		15.17		0.74
401	266		15.32		0.62	428	266		14.66		0.77
616	266		15.26		0.96	706	266		16.89		0.74
263	268		15.39		0.79	645	268	3- 142	16.01	0.06	0.58
467	270		13.91		1.06	358	271		15.30		0.66
531	271		14.03		0.74	561	272	3- 39	15.97	0.11	0.61
342	273		15.07		0.72	387	273		15.65		0.64
400	272		15.95		0.59	546	275	3- 34	16.43	0.10	0.69

TABLE 5. (continued)

x (pixels)	y (pixels)	Star ID	V(CTIO) (mag)	Δ (V) (mag)	V−R (mag)	x (pixels)	y (pixels)	Star ID	V(CTIO) (mag)	Δ (V) (mag)	V−R (mag)
400	272		15.95		0.59	546	275	3- 34	16.43	0.10	0.69
668	278	3- 141	16.14	0.08	0.58	319	279		16.31		0.69
539	280		15.09		0.69	552	280	3- 40	14.90		0.80
260	281	2- 1	15.74	0.16	0.98	382	281		15.82		0.57
373	283		14.44		0.76	392	283		13.73		1.08
403	284		15.06		0.75	619	284	3- 150	15.91	0.09	0.59
323	285		14.48		0.79	562	285	4- 1	16.82	0.07	0.71
189	286	1- 153	15.53	0.10	0.74	553	286		16.01		0.83
334	287		15.99		0.61	611	287	4- 101	15.49	0.09	0.50
398	288		15.90		0.63	410	288		15.45		0.63
369	288		15.56		0.74	420	288		13.81		0.65
709	291		14.24		0.86	231	292	1- 152	16.50	0.07	0.68
281	292	1- 42	16.87	0.12	0.70	288	292	1- 43	15.77	0.09	0.64
387	293		16.10		0.58	762	295		16.07		0.57
232	297	1- 151	16.03	0.21	0.61	515	297		16.34		0.61
412	299		15.81		0.58	399	302		14.40		0.82
298	300	1- 44	15.95	0.09	0.60	388	301		15.99		0.65
693	303		14.15		0.49	763	304		14.49		0.73
375	305		15.78		0.60	418	307		14.90		0.70
155	310		15.68		0.80	293	311	1- 39	15.34	-0.02	0.44
606	311	4- 104	16.90	0.06	0.75	639	311	4- 103	15.94	0.07	0.57
410	312		15.00		0.68	319	315		16.70		0.64
673	317		16.00		0.58	557	322	4- 9	16.51	0.07	0.69
601	324	4- 105	16.87	0.07	0.71	353	326		14.70		0.81
320	326	1- 31	15.96	0.10	0.62	372	328		16.22		0.65
534	329		16.52		0.63	736	330		16.46		0.64
309	331		15.17		0.78	291	332	1- 34	15.28	0.01	0.69
498	332		15.97		0.64	506	332		16.02		0.57
565	332	4- 10	15.43	0.09	0.73	385	333		14.96		0.78
325	333	1- 30	16.74	0.07	0.62	624	333	4- 106	16.57	0.08	0.73
253	336	1- 141	15.07	-0.01	0.73	670	336		15.97		0.67
299	337	1- 33	14.90	-0.04	0.80	587	342	4- 112	15.17	0.02	0.76
762	343		16.09		0.55	406	349		14.47		0.87
555	350	4- 12	15.60	0.07	0.61	395	355		15.73		0.83
385	364		15.59		0.60	542	366	4- 21	14.62	-0.03	0.82
532	367	4- 20	16.15	0.15	0.66	574	367	4- 119	16.59	0.14	0.60
378	368		15.53		0.74	129	369		15.53		0.51
570	370	4- 120	15.59		0.71	299	376	1- 20	16.69	0.02	0.69
235	378	1- 137	16.89	0.07	0.74	566	378	4- 121	16.81	0.06	0.72
635	378	4- 111	15.43	0.01	0.61	215	381	1- 135	16.39	0.10	0.80
689	381		16.07		0.56	668	383		15.94		0.72
655	387		16.60		0.67	353	388		15.04		0.81
387	390		15.94		0.58	588	397		15.90		0.61
736	399		16.43		0.62	561	406		15.04		0.69
755	416		16.24		0.57	629	417		16.53		0.65
723	420		16.06		0.76						

widths (using the average of the values at the two luminosities $K_0=-3$ and -4 mag given in Table 8) measured in the sample globular clusters (omitting NGC 7099, as the reddening is too low) in $(V-K)$, $(J-K)$, and $(B-V)$ with those expected if the entire effect is caused by patchy interstellar reddening or if it is caused exclusively by abundance variations. The allowed ranges for the color width ratios given in Table 9 are obtained from the uncertainties for the color widths given in Table 8. The last column of Table 9 gives the range in $E(B-V)$, $\delta[E(B-V)]$, as inferred from $\delta(V-K)$, divided by the mean reddening for the cluster.

In all cases and for all colors from B to K (with the single exception discussed below) the ratios of the color widths of the globular cluster giant branches are completely consistent with all the spreads arising from patchy interstellar reddening. No cluster behaves as though metallicity variations dominate the cause of the color spreads.

The $(J-K)$ data are least useful here. The reddening is small across that bandpass, and hence, if the widths are due to patchy interstellar reddening, they too will be small in the K, $(J-K)$ diagram. This is in fact what is observed (see Table 8). The only case which slightly violates the perfect agreement of interstellar reddening with the observed color spread ratios is that of $\delta(V-K)/\delta(J-K)$ in NGC 6624. Perhaps the uncertainties in the color widths have been underestimated, or the effect of field stars and/or AGB stars is becoming important given that the color widths, particularly $\delta(J-K)$, are now small.

To show exactly how much one can constrain δ[Fe/H] using the ratios of the color widths, Fig. 6 illustrates the situation for NGC 6528, the cluster with the largest reddening. The regime allowed by the observed color widths [$\delta(V\text{-}K)=0.64\pm0.05$ mag and $\delta(B-V)=0.23\pm0.04$ mag] is shown by solid lines for $(B-V)$ and dashed lines for $(V-K)$. The intersection of the two families of curves is the allowed region. The measured values in Table 8 agree with the predictions for no metallicity variations whatsoever, while at most δ[Fe/H]=0.35 dex is allowed by the uncertain-

TABLE 6. IR Photometry for NGC 6171.

x (pixels)	y (pixels)	J (mag)	σ(J) (mag)	K (mag)	σ(K) (mag)	Optical ID		x (pixels)	y (pixels)	J (mag)	σ(J) (mag)	K (mag)	σ(K) (mag)	Optical ID	
456	-58	12.29	0.05	11.57		1	235	454	-56	11.66	0.03	10.72	0.04	1	234
431	-48	14.06	0.07	13.32	0.04			441	-39	10.65	0.02	9.59	0.02	1	245
435	-38	14.19	0.05	13.63	0.02			453	-38	14.28	0.05	13.88	0.05	1	244
462	-35	10.34	0.02	9.24	0.01	1	243	468	-35	14.45	0.11	13.67	0.04		
439	-27	14.23	0.10	13.43	0.02			449	-26	12.15	0.07	11.31	0.04	1	246
443	-23	12.66	0.04	11.92	0.01	1	247	435	-20	13.40	0.03	12.76	0.02	1	248
160	5	9.61	0.02	8.43	0.05	1	E	221	39	11.59		10.67		1	146
198	63	14.49		13.76				287	63	13.09		12.34			
247	64	12.13		11.27		1	145	178	67	13.25		12.60			
272	76	14.06		13.61		V	12	162	91	12.78		11.89		1	142
167	98	14.75		13.85				298	100	13.47	0.03	12.67		1	191
93	105	11.35	0.01	10.35	0.02	1	Q	182	114	15.25	0.03	14.47			
239	121	13.45	0.04	12.82	0.01	1	144	75	122	15.09	0.03	14.28	0.04		
276	124	14.27	0.03	13.48	0.02			99	128	13.30	0.04	12.46		1	135
319	130	13.52	0.03	12.85		1	193	256	136	13.52	0.04	12.74	0.04	1	192
85	146	13.66	0.01	12.81		1	134	202	146	13.70	0.02	13.13		1	143
348	158	13.36	0.15	13.08		1	195	245	163	14.39	0.00	13.81			
499	173	13.32	0.11	13.01		1	254	285	178	13.50	0.01	12.88	0.02	1	197
273	178	13.29	0.01	12.51	0.02	1	198	294	188	13.29	0.04	12.49	0.02	1	196
426	193	13.01	0.05	12.44	0.02	1	210	279	195	14.02	0.01	13.28	0.02	1	199
167	199	14.80	0.01	14.03				467	201	13.42	0.04	13.11		1	209
363	206	14.07	0.02	14.06		V	15	293	220	14.03	0.07	13.28			
337	233	14.40	0.04	13.74	0.16			472	244	14.01	0.04	13.43		1	208
213	260	14.67	0.04	13.94				274	259	15.01	0.04	14.27	0.11	2	327
475	328	14.88	0.06	14.35				443	333	12.31	0.03	11.42	0.06	1	207
378	348	14.51	0.01	14.29				353	349	15.06	0.06	14.26		2	344
416	358	15.09	0.06	14.41		2	345	459	362	13.44	0.06	12.71	0.02	1	206
323	381	14.14	0.03	13.53	0.25										

TABLE 7. IR photometry in NGC 7099.

x (pixels)	y (pixels)	J (mag)	σ(J) (mag)	K (mag)	σ(K) (mag)	Optical	ID	x (pixels)	y (pixels)	J (mag)	σ(J) (mag)	K (mag)	σ(K) (mag)	Optical	ID
92	72	14.08	0.10	13.51	0.09	1	137	150	104	14.54	0.10	13.56	0.04	1	129
167	111	14.82	0.10	14.39	0.23			7	113	13.82	0.02	13.29	0.08	1	146
78	117	12.70	0.01	12.08	0.03	1	135	48	123	14.12	0.01	13.66	0.06	1	147
141	123	15.14	0.06	14.35	0.02	1	130	143	135	14.07	0.01	13.37	0.01	1	131
127	147	13.44	0.06	12.84	0.03	1	132	215	149	15.77		15.00			
84	153	13.48	0.01	12.85	0.03	1	134	337	155	13.48	0.01	12.96	0.08	1	112
313	156	12.40	0.00	11.71	0.07	1	110	197	156	14.06	0.02	13.52	0.11	1	126
231	167	13.75	0.14	13.09	0.04	1	120	162	168	15.11	0.07	14.73	0.18	1	128
285	186	13.69	0.01	13.15	0.10			89	188	14.63	0.00	14.10	0.00	1	150
33	190	14.97	0.00	14.39	0.11			244	190	13.05	0.02	12.40	0.08		
281	194	14.72		14.67				223	198	15.25	0.07	14.79			
236	201	15.24		14.70				267	205	12.52	0.01	11.92	0.06		
206	207	15.19	0.01	14.92				143	210	14.54	0.06	14.29	0.25		
160	215	14.17	0.11	13.71	0.02	V	1	-19	216	14.28	0.03	13.87	0.01		
82	226	14.91	0.01	14.35	0.01			76	228	13.06	0.01	12.46	0.02		
175	231	14.08	0.05	13.46	0.03			136	233	12.21	0.02	11.61	0.11		(14.03)
313	232	14.83		14.60				88	236	15.01	0.02	14.98	0.05	1	152
234	236	14.36	0.01	13.72	0.10			184	237	15.16	0.08	14.45			
173	238	13.08	0.05	12.46	0.05		(14.80)	256	245	13.92	0.03	13.49	0.03		
207	245	14.84	0.09	14.56	0.33	1	163	177	248	15.05	0.01	14.49			
240	250	13.87	0.04	13.55	0.06			256	249	14.35	0.06	14.13	0.05		
119	257	14.62	0.07	14.16	0.02			253	260	14.30	0.03	14.04			
347	260	14.76		14.27				308	262	15.02		14.93			
264	263	13.95	0.03	13.48	0.04			278	263	14.84		14.18			
62	265	13.79	0.01	13.31	0.04	1	157	127	266	14.23	0.05	13.67	0.06		
377	267	13.64		13.14	0.06	1	89	-11	269	13.92	0.00	13.37	0.03	1	166
287	269	11.23	0.02	10.58	0.02		(13.20)	132	269	14.88	0.06	14.65			
196	271	12.85	0.04	12.29	0.06		(14.42)	233	272	14.74		14.18	0.02		
299	272	13.42	0.03	12.87	0.06		(15.05)	351	275	13.70	0.01	13.01			
143	277	14.35	0.09	13.86				373	277	14.63		13.83	0.06		
252	279	13.76	0.06	13.24				308	279	12.40	0.01	11.76	0.06		
148	283	14.62	0.16	13.98	0.02			80	284	14.07	0.01	13.45			
172	286	14.59	0.09	13.90	0.04			188	291	14.63	0.01	14.71			
286	291	13.51	0.04	12.92	0.03		(15.13)	162	296	10.65	0.05	9.96	0.05		(12.79)
294	297	11.76	0.02	11.10	0.02		(13.59)	154	298	15.07	0.00	14.38			
186	299	12.56	0.08	11.94	0.07		(14.41)	127	301	13.81	0.12	13.21	0.08		
175	304	14.57	0.09	13.99	0.09			154	308	14.53		14.15	0.10		
216	308	12.81	0.08	12.17	0.10		(14.50)	75	309	13.61	0.00	12.88	0.03		
235	310	11.22	0.03	10.51	0.08		(13.12)	201	311	14.75		14.37			
156	313	11.33	0.04	10.67	0.05		(13.26)	-19	316	13.05	0.00	12.51	0.03	1	169
178	316	12.38	0.07	11.72	0.05		(14.10)	194	315	13.07	0.09	12.44	0.06		
200	318	15.12	0.09	14.83				281	318	13.52	0.12	12.91			
11	320	14.43	0.00	14.06		1	168	208	320	14.71	0.01	14.30			
368	320	14.93		14.36				171	321	14.13	0.01	13.65	0.08		
182	322	14.23		13.85				190	322	13.82	0.04	13.38	0.08		
278	322	13.62		13.14				222	324	13.55	0.09	13.01	0.11		
176	326	13.51	0.06	12.95	0.10			255	328	10.74	0.02	10.04	0.07		
274	326	13.05		12.48				276	328	12.90	0.08	12.29	0.08		
140	329	14.60	0.01	14.10	0.08			203	330	13.09	0.05	12.55	0.09		
262	331	13.11	0.08	12.49	0.06			161	331	12.63	0.03	11.96	0.07		
350	334	13.97		13.29	0.02			187	335	14.44	0.03	13.93			
322	335	10.22		9.47	0.06		(12.42)	251	337	13.39		12.81	0.13		
272	337	13.38		12.75				175	339	12.55		11.92	0.09		(14.23)
349	333	13.92	0.07	13.52				267	339	13.54	0.11	12.93	0.12		
188	342	11.59	0.02	10.88	0.07		(13.45)	198	345	11.49	0.04	10.77	0.08		(13.38)

TABLE 7. (continued)

x (pixels)	y (pixels)	J (mag)	σ(J) (mag)	K (mag)	σ(K) (mag)	Optical	ID	x (pixels)	y (pixels)	J (mag)	σ(J) (mag)	K (mag)	σ(K) (mag)	Optical	ID
354	351	13.80	0.09	13.26	0.08			165	351	12.73	0.02	12.01	0.09		(14.21)
315	354	13.44		12.72				296	357	12.79	0.01	12.16	0.14		
241	363	12.72	0.03	12.01	0.12			287	366	11.00	0.03	10.26	0.08		(12.83)
352	371	14.64		14.93				283	380	12.09	0.01	11.44	0.10		
350	393	10.51	0.04	9.81	0.04	1	17	224	380	13.87		13.13			
224	388	12.69	0.11	12.08				213	389	14.79	0.08	14.11			
228	395	11.37	0.10	10.76	0.02			222	398	13.74	0.01	13.08	0.03		
179	399	12.28	0.11	11.64				199	403	14.58	0.06	13.89	0.12		
339	403	14.14	0.01	13.44				162	410	15.49		14.66			
195	413	13.18	0.10	12.52	0.05			212	417	12.75	0.08	12.07	0.03		
154	418	13.13	0.09	12.49	0.03			227	419	15.02	0.23	14.46	0.24		
96	425	14.73	0.07	14.48	0.08			224	425	14.96	0.09	14.34	0.07		
324	426	15.13	0.04	14.86	0.21			281	427	14.28	0.12	13.67	0.15		
251	432	14.95	0.17	14.30	0.26			257	432	14.09	0.05	13.40	0.11		
301	434	13.71	0.07	13.01	0.07			178	435	14.27	0.04	13.70	0.04		
169	437	11.30	0.06	10.56	0.04		(13.20)	100	437	14.70	0.08	14.15	0.28		
149	445	13.74	0.08	13.13	0.05			203	446	15.07	0.06	14.46	0.08		
256	449	14.57	0.10	13.97	0.11			92	449	13.92	0.08	13.41	0.10		
167	463	12.81	0.04	12.21	0.04			220	464	13.70	0.13	13.09	0.12		
295	465	15.72		14.96	0.04			160	480	13.66	0.04	13.09	0.04		
272	483	15.60	0.03	14.98				160	484	14.88		14.11			
120	485	14.43	0.14	13.83	0.12			129	487	15.14	0.04	14.42			
118	487	14.45	0.07	13.78	0.02			302	489	13.85	0.03	13.20	0.06		
140	501	11.51	0.03	10.83	0.08			180	502	13.36	0.02	12.77	0.04		
232	503	11.41	0.02	10.68	0.03		(13.31)	152	508	13.15	0.05	12.55	0.04		
103	529	11.94	0.06	11.28	0.04	1	32	157	530	13.82	0.03	13.17	0.03	1	35
292	532	15.23	0.06	14.80	0.13			316	533	14.62	0.03	13.95	0.03		
130	536	15.06	0.03	14.93	0.05	1	33	136	540	13.68	0.02	13.10	0.04	1	34
282	562	14.81	0.01	14.44	0.03	1	48	285	570	14.66	0.03	14.23	0.08	1	47
283	577	14.03	0.02	13.43	0.01	1	46	186	586	15.43	0.00	14.73	0.02	1	37
129	594	15.56		14.75				313	600	15.22	0.05	14.69	0.12	1	56
217	609	14.37	0.01	13.86		1	40	318	615	13.44	0.01	12.79	0.04	1	57
252	615	15.66		14.84				308	670	13.90	0.10	13.36	0.12	1	58

ties in the color widths. If the uncertainty in $\delta(B-V)$ could be reduced, the upper limit on δ[Fe/H] could be made much lower.

For clusters with low interstellar reddening, a small upper limit to the range in $V-K$ along the giant branch is a very effective way to constrain internal metallicity variations. Equation (7) of Frogel *et al.* (1983a) shows that if $\delta(V-K)$ <0.10 mag, an easily measured value in the absence of differential reddening, then δ[Fe/H]<0.07 dex. This is the case for NGC 7099.

Note that $\delta(B-V)$ as deduced from $\delta(V-K)$ assuming only patchy interstellar reddening is contributing [which number is always close to the measured $\delta(B-V)$ value] implies a variation in the reddening (measured in magnitudes) of 30% to 40% across small fields within a globular cluster. Given the modest reddening (0.3–0.6 mag) for these objects, that is rather surprising. The ISM is very patchy on very small spatial scales.

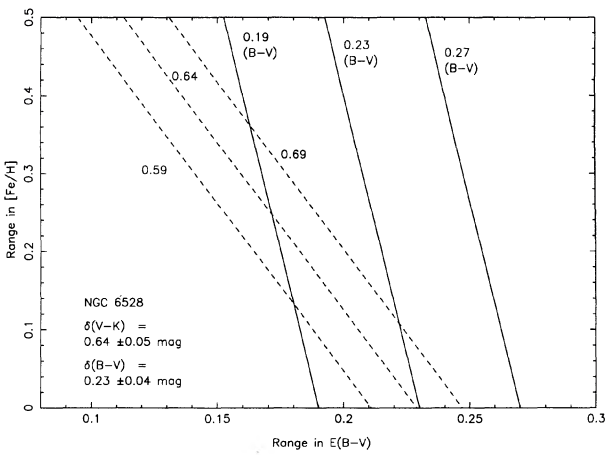

FIG. 6. The permitted regime of $B-V$ or $V-K$ color and range in [Fe/H] that match the observed $\delta(B-V)$ or $\delta(V-K)$ color spreads in NGC 6528 is shown. The intersection of the two families of curves is the permitted region.

4.2 The Colors of the Giant Branches

Frogel *et al.* (1983a) demonstrated that the color of the giant branch of a globular cluster in the infrared depends primarily on the metallicity of the cluster. Although in a theoretical $\log(T_{\rm eff})$–$M_{\rm bol}$ plane, the offset with metallicity is roughly independent of height along the giant branch (Green *et al.* 1987), this translates in the observational plane into increasingly larger changes in color as the giant branch gets cooler near the tip. Thus, we use the measurements of color of the giant branch in $(J-K)_0$ and $(V-K)_0$ made at $M_{K_0}=-5$ mag. Table 10 gives measurements of the mean color of the giant branch in the five sample globular clusters at $M_{K_0}=-5$ and -4 mag, together with the adopted reddening and distance moduli.

Colors for the giant branches of three calibrating clusters, 47 Tuc, M13, and M92, are also given, based on the data in Cohen *et al.* (1978) or in Frogel *et al.* (1981). The ridge lines in $(V-K)_0$ are in fact tabulated in the last reference. We have corrected the 47 Tuc ridge lines for the different assumption regarding the absolute magnitude of the horizontal branch made here as compared to that adopted by Frogel *et al.* (1981).

To our sample, we add the very metal rich galactic globular cluster NGC 6553, with infrared photometry of the upper giant branch by Davidge & Simons (1994) and visual photometry from Hartwick (1975).

We use a weighting of 3 for abundance from $(V-K)_0$ as compared to that from $(J-K)_0$ because of the much lower sensitivity of the mean $(J-K)$ color of a cluster giant branch at a fixed M_{K_0} to abundance changes. Furthermore, we must extrapolate to higher metallicities than 47 Tuc even though we lack any calibrating clusters more metal rich than 47 Tuc. Since the $(J-K)$ gradients are relatively small, we used the gradients in color between M13 and 47 Tuc at $M_{K_0}=-5$ to extrapolate to metallicities higher than that of 47 Tuc, assumed to be at [Fe/H]$=-0.71$ dex. When applied to $(V-K)$, this leads to problems, in that the giant branches, particularly near their tips, become acceleratingly redder as the metallicity increases in a nonlinear way, and we would deduce abundances which significantly exceed solar metallicity for the most metal rich clusters studied here. To minimize this effect, we use NGC 6171, whose metallicity can be well established through the procedure described above, as its [Fe/H] lies between that of 47 Tuc and that of M13. For the globular clusters more metal rich than 47 Tuc, we then use the gradients determined by comparing $(V-K)_0$ at a fixed M_{K_0} between the NGC 6171 giant branch and that of 47 Tuc. That gradient Δ[Fe/H]/$\Delta(V-K)_0$ is about 30% smaller than if the 47 Tuc giant branch were compared to that of M13. We do not know how much the gradient continues to decrease as [Fe/H] increases still further.

Several attempts have been made to determine the metallicity of these very metal rich clusters. Two of these clusters were included in Frogel *et al.*'s (1983a) analysis of infrared photometry for the brightest part of the giant branch, two are included in Cohen's (1983) low-dispersion spectroscopic analysis of individual stars, all are included in Zinn's (1980) study of Ca II absorption in the integrated light, and three are included in Armandroff & Zinn's (1988) analysis of Ca II absorption in the infrared triplet in the integrated light.

Table 11 summarizes the situation. The abundances derived by various authors have been linearly shifted in an appropriate way to force the same abundance for 47 Tuc, -0.71 dex. Typical errors cited for each determination are ±0.15 dex, but this does not include any calibration or scale error. While the lower end is fixed by 47 Tuc, which has been extensively studied by many people, the extension in abundance above 47 Tuc is poorly calibrated in all of these analyses.

Given the magnitude of the uncertainties in all the abundance determinations, and considering that none of the schemes is well calibrated for objects more metal-rich than 47 Tuc, the results are encouraging. All the schemes rank the clusters in metallicity in the same order. However, we have a small problem (not more than 0.4 dex in total) with the details of the abundance values for the three metal rich clusters, in that compared to the prior analyses. NGC 6528 and NGC

TABLE 8. Observed width of the giant branch for five globular clusters.

Cluster	$E(B-V)$ (mag)	$\delta(B-V)$ ($M_{K_0}=-3$)	$\delta(B-V)$ ($M_{K_0}=-4$)	$\delta(J-K)$ ($M_{K_0}=-3$)	$\delta(J-K)$ ($M_{K_0}=-4$)	$\delta(V-K)$ ($M_{K_0}=-3$)	$\delta(V-K)$ ($M_{K_0}=-4$)
NGC 6528	0.62	0.23:	0.23:	0.17	0.12	0.64	0.63
NGC 5927	0.46	0.13	0.13	0.08	≤0.05	0.55	0.48
NGC 6624	0.28	0.08	0.08	0.08	0.10	0.25	0.22
NGC 6171	0.33	0.13	0.13	0.05	≤0.05	0.33	0.25
NGC 7099	0.05	≤0.05	≤0.05	≤0.08	≤0.08	≤0.10	≤0.10

TABLE 9. Predicted versus observed ratios for color widths.

Cluster	$E(B-V)$ (mag)	$\frac{\delta(V-K)}{\delta(J-K)}$	Allowed Range	$\frac{\delta(V-K)}{\delta(B-V)}$	Allowed Range	$\frac{\delta[E(B-V)]}{E(B-V)}$
NGC 6528	0.62	4.3	(3.1, 6.3)	2.8	(2.2, 3.6)	0.37
NGC 5927	0.46	8.5	(5.2, 18.3)	3.9	(2.9, 5.5)	0.40
NGC 6624	0.28	2.7	(1.7, 4.7)	3.0	(1.8, 5.6)	0.31
NGC 6171	0.33	7.3	(4.2, 16.5)	2.2	(1.6, 3.3)	0.31
Expected:						
$\delta(B-V)$		5.4		2.8		
δ[Fe/H]		4.1		8.6		

TABLE 10. Mean colors of giant branches of globular clusters.

Cluster	$E(B-V)$ (mag)	[Fe/H] (dex)	Distance Modulus (mag)	$\langle(J-K)_0\rangle$ ($M_{K_0}=-4$)	$\langle(J-K)_0\rangle$ ($M_{K_0}=-5$)	$\langle(V-K)_0\rangle$ ($M_{K_0}=-4$)	$\langle(V-K)_0\rangle$ ($M_{K_0}=-5$)
NGC 6528	0.55	−0.23	14.42	0.92	1.03	3.85	4.62
NGC 5927	0.46	−0.31	14.17	0.82	0.92	3.27	3.88
NGC 6624	0.28	−0.37	14.18	0.98	1.05	3.21	3.73
NGC 6171	0.33	−0.99	13.81	0.85	0.96	2.98	3.46
NGC 7099	0.05	−2.13	14.29	0.68	0.75	2.57	2.86
Additional Cluster:							
NGC 6553	0.78	−0.28	13.16	0.89	1.03	3.60	4.63
Calibrating Clusters:							
47 Tuc	0.04	−0.71	13.03	0.85	0.94	3.26	3.78
M13	0.02	−1.65	14.13	0.70	0.79	2.70	3.08
M92	0.02	−2.24	14.33	0.67	0.74	2.57	2.83

TABLE 11. Abundances of metal rich globular clusters.

Cluster	$[Fe/H]_Z$ (dex)	$[Fe/H]_{AZ}$ (dex)	$[Fe/H]_C$ (dex)	$[Fe/H]_{FCP}$ (dex)	$[Fe/H]_{CS}$ (dex)
NGC 6528	−0.04	−0.25	...	...	+0.10
NGC 5927	−0.23	−0.30	−0.12	−0.30	−0.66
NGC 6624	−0.31	−0.30	...	...	−0.58
NGC 6171	−0.96	...	−0.93	−1.04	−1.00
NGC 7099	−2.26	...	...	...	−2.15
Additional Cluster:					
NGC 6553	−0.03	...	−0.31	(−0.30)	+0.10

Normalized to $[Fe/H]_{47\ Tuc}=-0.71$ dex

6553 appear to be too metal rich, while NGC 5927 and NGC 6624 appear too metal poor, relative to 47 Tuc. We remark that Kuchinski *et al.* (1994) have also found that NGC 5927 in the infrared is essentially identical to 47 Tuc, and is not much more metal-rich than 47 Tuc.

The measurements of integrated light spectral features are insensitive to choices of distance or reddening, while those based on giant branch properties or on spectroscopic analysis of individual stars do depend on the choice for these parameters. The horizontal branch apparent V magnitudes are well determined, even for these crowded and metal rich clusters in very crowded fields, from our new Tololo photometry or from Ortolani *et al.* for NGC 6528, and no error larger than 0.10 mag is allowed. Numerical tests indicate that if the true distance modulus is overestimated by 0.4 mag, the deduced abundance of the globular cluster from the infrared colors of its giant branch is underestimated by 0.35 to 0.55 dex. Since the allowed errors in the horizontal branch apparent magnitude are much smaller than 0.4 mag, this effect is probably not contributing in a significant way. Similarly, changing the adopted M_V calibration for the RR Lyraes to any other plausible choice will not do much to the deduced abundances, since everything is measured differentially with respect to the calibrating clusters.

Different choices for the interstellar reddening will not only affect the giant branch colors directly, but will also affect the deduced distance modulus. Numerical tests of this case indicate that if $E(B-V)$ is reduced by 0.10 mag, and the distance modulus adjusted appropriately, the metallicity of the globular cluster as inferred from the colors of its upper giant branch stars is increased by 0.16 dex.

Another potential cause of uncertainty is the absolute calibration of our infrared photometry. By comparison of our measurements with previously published and recent unpublished infrared photometry, we have shown above that these errors do not exceed 0.10 mag at K. This translates into Δ[Fe/H]$\approx$0.12 dex for a very metal rich globular cluster, which is smaller than the discrepancies in abundance that we are discussing.

One might therefore suspect our small problems with NGC 5927 and NGC 6624 to be caused by a combination of the allowable small error in apparent magnitude of the horizontal branch (0.10 mag) and the distance modulus. One might also try slightly decreasing the reddening, although that of NGC 6624 is so small already [$E(B-V)=0.31$ mag] that no significant decrease seems plausible. The extrapolation we have used of the giant branch color changes with metallicity beyond 47 Tuc to such metal rich objects as NGC 6528 and NGC 6553 is such that the metallicity of those two objects has probably been slightly overestimated.

There is no completely satisfactory solution for reproducing from our infrared photometry the previously determined metallicities for these three globular clusters.

We summarize our conclusions as follows:

(1) The ordering of the metallicities we have derived for the observed clusters is correct, but there are some problems with the detailed numerical values. NGC 5927 and NGC 6624 appear to be more metal poor, and much closer to 47 Tuc in metallicity, than was previously believed. On the other hand, if our adopted value for the gradient Δ[Fe/H]/$\Delta(V-K)_0$ is correct (and recall that we were forced to extrapolate in color considerably redder than the giant branch of 47 Tuc, the most metal rich calibrating cluster), then NGC 6528 and NGC 6553 may be more metal rich than was previously believed.

(2) A spread in the giant branch of $\delta(V-K)\approx$0.5 mag at a fixed K magnitude is seen in NGC 5927. A spread of about 0.6 mag is seen in NGC 6528. If these were due solely to differential reddening, $\delta E(B-V)$ would be about 0.20 mag in NGC 5927 and about 0.24 mag in NGC 6528. (In NGC 5927, a deliberate effort was made to observe in an area found by previous optical studies to have relatively uniform absorption.) The range of $V-K$ is smaller in the other clusters observed.

These numbers are in good agreement with estimates from previous optical studies of the magnitude of the differential reddening within the clusters.

(3) The observed spread in various colors along the giant branch for the heavily reddened globular clusters in our sample is consistent with patchy interstellar reddening strongly varying on a small spatial scale. No abundance variations within clusters are required to match the observations.

(4) The observed spreads of the upper giant branch in these metal rich globular clusters at various colors confine the internal range of metallicity. This must be less than 0.2 dex in NGC 5927 and less than 0.1 dex in NGC 7099. The spread in $V-K$ color at a fixed K magnitude is a strong constraint on [Fe/H] variations within a cluster.

Eric Persson and his team built the infrared camera in use at the Las Campanas Observatory. We are grateful to him and to Jay Frogel for several useful discussions. We are grateful to the Cerro Tololo Inter-American Observatory for the service observing of CCD images in V and R of NGC 5927 and of NGC 6624 using the Yale telescope. Keith Matthews helped with the infrared observations at the 200 in. telescope at Palomar Mountain. ECS was partially supported by a stipend from the National Physical Science Consortium.

REFERENCES

Alcaino, G., & Liller, W. M. H. 1980, AJ, 85, 1330
Armandroff, T. E., & Zinn, R. 1988, AJ, 96, 92
Bolte, M. 1987, ApJ, 319, 760
Cohen, J. G. 1983, ApJ, 270, 654
Cohen, J. G. 1992, ApJ, 400, 528
Cohen, J. G., Frogel, J. A., & Persson, S. E. 1978, ApJ, 222, 165
DaCosta, G. S., Mould, J. R., & Ortolani, S. 1984, ApJ, 282, 125
Davidgè, T. J., Harris, W. E., Bridges, T. J., & Hanes, D. A. 1992, ApJS, 81, 251
Davidge, T. J., & Simons, D. A. 1991, AJ, 101, 1720
Davidge, T. J., & Simons, D. A. 1994, AJ, 107, 240
Dickens, R. J. 1972, MNRAS, 157, 299

Elias, J. H., Frogel, J. A., Matthews, K., & Neugebauer, G. 1982, AJ, 87, 1029
Frogel, J. A., Cohen, J. G., & Persson, S. E. 1983a, ApJ, 275, 773
Frogel, J. A., Persson, S. E., & Cohen, J. G. 1981, ApJ, 246, 842
Frogel, J. A., Persson, S. E., & Cohen, J. G. 1983b, ApJS, 53, 713
Green, E. M., Demarque, P., & King, C. R. 1987, The Revised Yale Isochrones and Luminosity Functions (Yale University Observatory)
Hartwick, F. D. A. 1975, PASP, 87, 77
Jones, R. V., Carney, B. W., Storm, J., & Latham, D. W. 1992, ApJ, 386, 646
Kuchinski, L., Frogel, J. A. F., Terndrop, D., & Persson, S. E. 1994 (in preparation)
Liu, T. X., & Janes, K. A. 1990, ApJ, 360, 561
Liller, M. H., & Carney, B. W. 1978, ApJ, 224, 383
Menzies, J. 1974, MNRAS, 169, 79
Ortolani, S., Barbuy, B., & Bica, E. 1991a, ApJ, 249, L31
Ortolani, S., Bica, E., & Barbuy, B. 1991b, A&AS, 92, 441
Persson, S. E., West, S. C., Carr, D. M., Sivaramakrishnan, A., & Murphy, D. C. 1992, PASP, 104, 204
Peterson, C. 1993, in The Structure and Dynamics of Globular Clusters, edited by S. Djorgovski and G. Meylan (ASP)
Sandage, A. R., & Katem, B. 1964, ApJ, 139, 1088
Sawyer Hogg, H. 1973, Publications of the David Dunlop Observatory, 3
Stetson, P. B. 1987, PASP, 99, 99, 191
van den Bergh, S., & Younger, F. 1979, AJ, 84, 1305
Zinn, R. J. 1980, ApJS, 42, 19
Zinn, R., & West, M. 1984, ApJS, 55, 45